IEEE Access
Multidisciplinary | Rapid Review | Open Access Journal

Received 15 April 2023, accepted 4 May 2023, date of publication 9 May 2023, date of current version 19 May 2023.

Digital Object Identifier 10.1109/ACCESS.2023.3274701

RESEARCH ARTICLE

The Demagnetization Phenomenon in PM Machines: Principles, Modeling, and Design Considerations

FARSHID MAHMOUDITABAR[1], ABOLFAZL VAHEDI[2], (Senior Member, IEEE), AND FABRIZIO MARIGNETTI[3], (Senior Member, IEEE)

[1]School of Engineering, Newcastle University, NE1 7RU Newcastle upon Tyne, U.K.
[2]Electrical Engineering Department, Iran University of Science and Technology, Tehran 13114-16846, Iran
[3]Department of Electrical and Information Engineering "Maurizio Scarano" (DIEI), University of Cassino and South Lazio, 03043 Cassino, Italy

Corresponding author: Fabrizio Marignetti (marignetti@unicas.it)

This work was supported in part by the Innovation Agreement Contract "Ulisse, sUstainable rolLIng Stock to inSpire the nExt," in part by the Decree of the Ministry of Enterprises and Made in Italy (December 31, 2021), and in part by Hitachi Rail Spa.

ABSTRACT Permanent Magnet (PM) machines have attracted much attention due to their high power-torque density, high efficiency, high dynamic response performance, high power factor, and simple structure. Even though there are some uncertainties about their reliable chain supply, PM machines still are the first choice for high-performance applications. Therefore, paying attention to the development and improvement of the performance of these types of electric machines is of great importance. One of the challenges of the PM machines is their vulnerability to Irreversible Demagnetization (ID), especially for applications such as Electric Vehicles (EV), in which the working temperature and Magnetic Motive Force (MMF) produced by stator winding are higher than in conventional applications. Therefore, the ID phenomenon must be regarded as a leading design and control parameter for PM machine designers. The ID can be defined as an irreversible reduction of the remnant flux density of the PM or the EMF of the PM machine due to severe temperature conditions, high external Demagnetization Field (DF), or non-proper design of PM machines, resulting in degradation in performance of the PM machines. The lack of a good source that gives a deep inside into this phenomenon in designing and developing PM machines encourages the author to conduct a comprehensive literature review. For proper design of the PM machines in terms of ID, it is necessary to consider four critical steps, i.e.: (a) accurate non-linear modelling of the PM demagnetization curve, (b) analytical model taking into account local ID, (c) geometry optimization methods targeting ID, (d) accurate experimental testing to evaluate the ID fault-tolerant capability of the manufactured PM machines. In this paper, the above four aspects are surveyed exclusively, and the advantages and disadvantages of the existing methods in these areas are highlighted. Furthermore, design tips towards the design of ID fault-tolerant PM machines and other research opportunities to enhance the reliability of PMs machines are also presented.

INDEX TERMS Demagnetization, optimization, fault-tolerant design, permanent magnet.

I. INTRODUCTION

In recent years, PM motors have been widely used in various industries due to their excellent performance characteristics, such as high power-torque density, high efficiency, easy construction, and high reliability. Therefore, paying attention to the development and improvement of the performance of these types of electric machines is of great importance. From the perspective of reliability and durability, PM machines are suffering from the phenomenon of ID, especially for applications such as EV, in which the working temperature and MMF produced by stator winding are higher than in conventional applications [1], [2]. Therefore, the ID phenomenon must be considered among the leading design and control parameters. In fact, in the case of ID, the electromagnetic performance of the PM machines is weakened; therefore, a higher current is needed for a constant output torque. Consequently, a further increase in the working temperature will have happened.

The associate editor coordinating the review of this manuscript and approving it for publication was Feifei Bu.

Many papers deal with the phenomenon of ID and perform valuable tips and instructions to accurately model, design, and optimize the PM machines to avoid ID [3], [4], [5], [6], [7]. Currently, no well-organised source exists for the proper definition of ID, its modelling methods, and design tips to avoid ID. Only three review papers deal with the ID analysis of the PM machines, and all focus on ID fault diagnosis techniques. In [8] and [9], the available methods for ID fault detection of the PMSM machines were presented. In [10], Different modelling techniques for ID fault diagnosis of different types of PM machines are compared. Also, the proposed techniques for ID fault diagnosis under stationary and non-stationary conditions are summarized and compared.

For proper design of the PM machines in terms of ID, it is necessary to consider four key issues, namely: the non-linear modelling of the PM demagnetization curve, the analysis method, which must be capable of taking into account local ID, the geometry optimization methods capable of considering ID, and the choice of an accurate experimental test setup to evaluate the ID fault-tolerant capability of the manufactured PM machines. The contributions of this paper consist of a systematic survey of these four aspects and a comparison of the advantages and disadvantages of the methods used in these areas. Furthermore, design tips towards the ID fault-tolerant design of PM machines are presented. Also, other research opportunities to enhance the reliability of PMs machines are presented.

A. PM MODEL

The initial step in the investigation of ID in PM machines is the proper definition of the $B-H$ curve of the PM, which describes the demagnetization curve, including the knee point [11]. Defining the $B-H$ curve of the PM by conventional B_r and μ_r parameters is not accurate and inapplicable for ID analysis. Generally, four models, namely the limited model, the Linear Model (LM), the Exponential Model (EM), and the Hysteresis Model (HM) are utilized for the definition of the $B-H$ curve of the PM [12]. In recent years, some developed versions of these models are introduced to consider the temperature variations and increase the modelling accuracy [13], [14], [15], [16]. There are some attempts to compare these methods in the literature, but these papers only focused on three or four types of models [12], [17], [18].

B. ID ANALYSIS MODEL

Considering the proper ID analysis model can significantly influence the accuracy of the ID results. There are analysis models for the investigation of the ID of the PM machines including FEM [19], Magnetic Equivalent Circuit (MEC) [20], Maxwell's equation [21], Field Reconstruction Model (FRM) [22], Distributed lumped Parameter Model (DLPM) [23], etc. These methods were compared in [10] in terms of fault diagnosis techniques. The given comparison is developed in this paper to give a better insight into modelling aspects. These analysis models used for the treatment of the ID phenomenon will be discussed in detail in section IV.

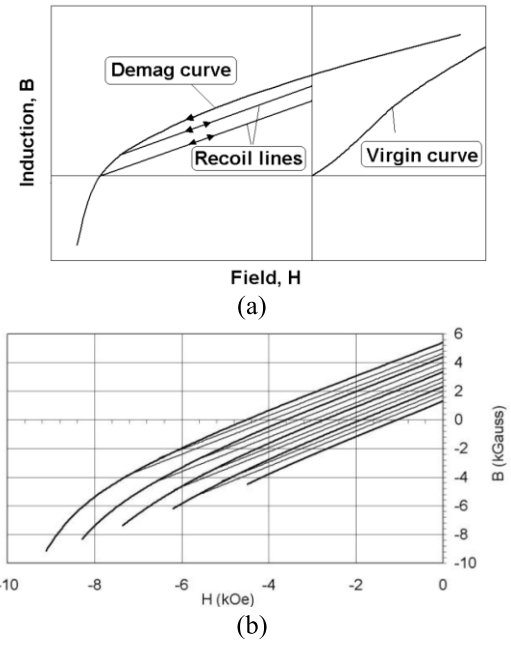

FIGURE 1. (a) Demagnetization curve and recoil lines of the permanent magnet and (b) Major and minor $B-H$ curve [34].

C. DESIGN OPTIMIZATION CONSIDERING ID

The essential step in the design of the PM motor is geometry optimization to achieve the desired output responses. One of these output responses is the ID fault-tolerant capability. The solutions to eliminate the risk of ID are 1. reducing the eddy current loss of the PMs to decrease the working temperature [24], [25], 2. Remove or replace the demagnetized area [26], [27], 3. Optimizing the structure of the magnetic circuit to protect the PMs against external DF [28], and 4. Considering the ID in the intelligent design optimization process [1], [29].

D. EXPERIMENTAL VERIFICATION TO EVALUATE TOLERABILITY AGAINST ID

To evaluate the accuracy of the ID analysis method and optimum design performance, it is necessary to use the experimental results. But, in the case of ID analysis, little attempt has been made, due to the destructive nature of ID experimental analysis. In most cases, to investigate the effect of ID, using a drill or other device, a part of PM was removed then by analyzing the PM machine's signals the ID fault and its severity are detected [3], [30], [31]. This method does not present the actual conditions of ID because the ID occurred partially over all of the PMs. The second method is based on heating the motor and injecting high-amplitude currents or SC conditions to create ID conditions [32], [33]. These methods present the real ID conditions compared to the first one.

This paper is composed of seven sections to address the above-mentioned steps. First, the ID-generating factors, and their impacts on the machine performance for different types of PMs are discussed. In section III, different PM model for

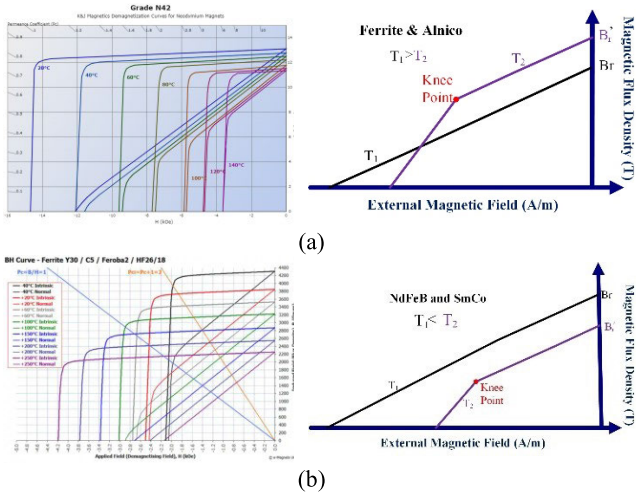

FIGURE 2. The effect of temperature on the B-H curve of the PMs (a) Ferrite and Alnico [38] (b) NdFeB and SmCo [39].

ID analysis is discussed. Section IV presents the ID modelling procedure and ID analysis model. Section V gives a literature review on design optimization of PM machines considering ID. Newcomers in the field of PM machine design must get familiar with different aspects of ID analysis and experimental methods for modelling the ID, these aspects are given in section VI. Finally, some design tips to avoid ID and some suggestions are presented for further research in this area.

II. DEMAGNETIZATION PRINCIPLES

The ID can be defined as losing the remnant flux density of the PM or losing the EMF of the PM machine. Which results in deration in performance of the PM machines. In other words, in the nominal condition, the PM has a specific value of the remnant flux density of B_r and the induced open voltage at the terminal of the machines will be E_{oc}. Working of the PM machines in the severe temperature conditions or high external DF led to ID which results in losing the initial magnetic properties of the PMs. As a result, the relative drop in the E_{oc} happens and the machine's overall performance will be affected and weaken.

The ID is completely dependent on the working point of the PM and demagnetization curve (second quadrant of the $B-H$ or $M-H$ curves). While the $B-H$ curve is known as the normal curve of the magnet which describes the relationship between the magnetic flux density B and magnetic field intensity H and the $M-H$ curve is known as the intrinsic curve which illustrates the relationship between magnetization M and H. The relation between the normal and intrinsic curve is defined as $B=\mu_0(H+M)$. The normal curve shows the magnetic field from the combination of the applied field and the PM, while the intrinsic curve shows only the magnetic field of the magnet [35], [36]. In the case of ID, the PM will be working on a minor loop of the $B-H$ curve. As it shown in Fig. 1, the minor loop is approximated by a recoil line that can be built based on the original major/minor $B-H$ curve [34].

The parameters influencing the ID are the working temperature, the external DF, the load line of the PM, and self-demagnetization. The comparison of the knee point and the working point of the PM is a criterion for the analysis of ID. The working point below the knee point is corresponding to ID. The working point of the PMs is obtained from the intersection of the demagnetization curve and the PM's load line. The description of the influential factors on ID is as follows.

A. TEMPERATURE

To study the effect of temperature on ID, it is necessary to divide the PMs into two groups of PMs with negative and positive Coercive Force Thermal Coefficient (CFTC). The negative CFTC indicates that with increasing the temperature the risk of ID increases and the positive one has the inverse effect. The negative CFTC is corresponding to NdFeB and SmCo magnets while the positive one is corresponding to Alnico and Ferrite magnets [37]. The actual B-H curve of both groups and simplified curve at two temperatures of T_1 (room temperature) and T_2 (high temperature in case of negative CFTC PMs and low temperature in case of positive CFTC PMs) are illustrated in Fig. 2. At room temperature, the knee point does not appear in the B-H curve of both groups. For negative CFTC magnets (Fig. 2(a)), with increasing temperature, the knee point appears on the B-H curve. While, for the positive CFTC magnets (Fig. 2(b)), with decreasing temperature, the knee point appears on the B-H curve. The ID should be investigated in the worst working condition. So, the worst working condition for negative and positive CFTC magnets are corresponding to the highest and lowest temperatures, respectively.

B. EXTERNAL DEMAGNETIZATION FIELD

As shown in Fig. 3(a), in the absence of the DF, P_0 corresponds to the working point of the PM, which is above the knee point. The load line of the PM is moved to the left by applying an external DF. It can cause two conditions:

1) EXTERNAL DF $<$ H_D

In this condition, the magnetic flux density of P_1 is higher than the B_{knee}. Therefore, if the external DF is removed, the PM can recover its initial B_r. This state is called reversible demagnetization.

2) EXTERNAL DF $>$ H_D

In this condition, the working point of the PM is moved to point P_2. In this case, the PM cannot recover its initial B_r. Therefore, the PM returns to a recoil line that has a slope like the demagnetization curve above the B_{knee}. The slope of the recoil line is called permeability, which is an intrinsic property of the PM material. Therefore, the PM returns to a lower residual flux density B_r'' and loses some of its magnetic properties. This state is called ID [40].

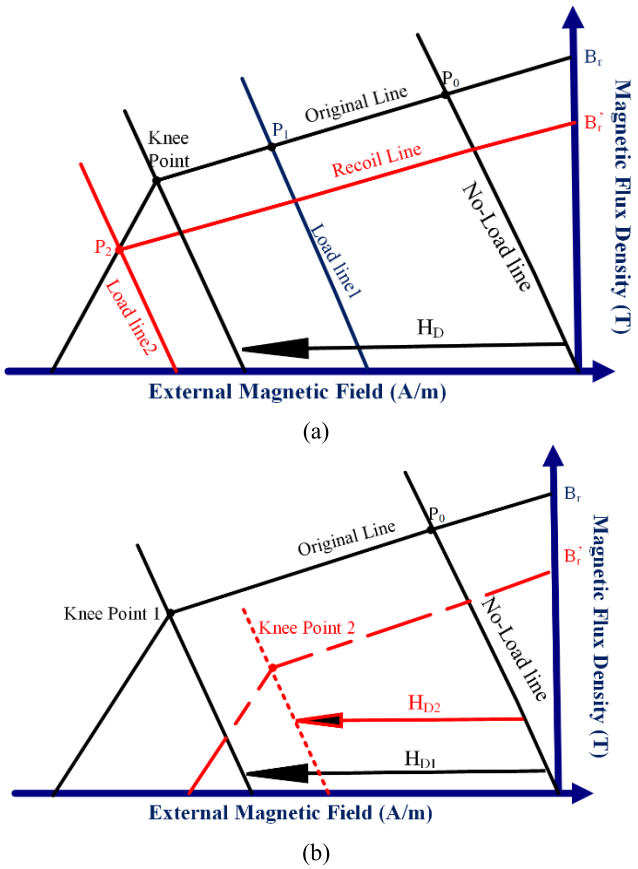

FIGURE 3. (a) The effect of armature reaction on ID (b) the effect of temperature on the required external DF for the NdFeB magnet.

The previous threshold for external DF and knee point were corresponding to the temperature of T_1. For NdFeB and SmCo magnets, with decreasing the temperature ($T_2 < T_1$), these thresholds will be changed. The required DF is increased, and the knee point value is decreased. Therefore, as was shown in Fig. 3(b), for these types of PMs, at a lower temperature (T_2), the risk of ID is significantly decreased.

An example of the high external DF in the PM machines is corresponding the dynamic operation of the PM machines. The dynamic operation of the PM machines is corresponding to over-load condition, acceleration in PM machines utilized in EV application, cooling system failure, etc. The relation between these dynamic operation and ID of the PM machines can be completely explained by Fig. 3 as follows:

1. Higher Current due over-load or acceleration: As shown in Fig. 3 (a), the load line of the magnet is shifted to left due to applied external demagnetization field. If the applied external demagnetization field due to over-load and acceleration current of the PM machines exceeds the acceptable value of H_D (criteria for ID), the ID will be occurred.
2. High working temperature due to over-load, acceleration, and cooling system failure: As shown in Fig. 3 (b), with increasing the working temperature of the PMs, the acceptable criteria for external demagnetization field will be reduced from H_{D1} to H_{D2} due to changes in the magnetic properties of the PM. In this condition, if the intersection of the load line of the magnet and Second quadrant of the curve located below the knee point, the ID will be occurred. Also, it should be noticed that the constant of the temperature rise of the PM machines are high. Therefore, we should not expect the higher difference in the working temperature of the machine in the acceleration condition.

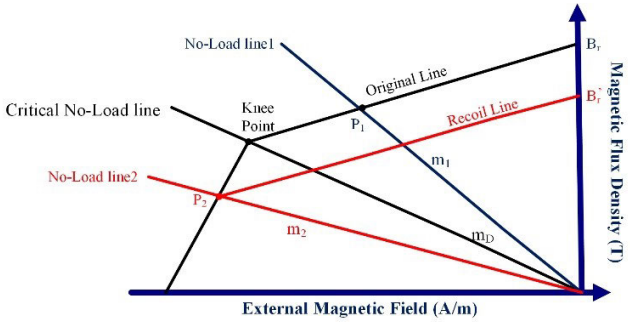

FIGURE 4. The effect of load line on the ID.

C. LOAD LINE OF THE MAGNET

Another important factor in the ID of the PM machines is the effect of the slope of the PM's load line. The load line of the magnet is calculated by writing Ampere's circuital law along the magnetic flux path of the PM. According to Fig. 4, based on the slope of the load line two conditions can happen:

1) THE SLOPE OF THE LOAD LINE $< m_D$

if the load line of the magnet is the L_1, clearly, the working point of the magnet (P_0) is above the knee point and the ID will not occur.

2) THE SLOPE OF THE LOAD LINE $> m_D$

The working point of the magnet is P_1, which is below the knee point, and ID will occur.

Fig. 4 illustrates the importance of designing PM machines from the point of view of the load-line slope. The PM motor designers should consider the highest working temperature to select design parameters properly. Therefore, improper selection of the design parameters will lead to ID at a high working temperature, even without external DF.

D. SELF-DEMAGNETIZATION

In addition to the external magnetic field and temperature, there is one more reason for declining the magnetic properties of the magnet material which is self-demagnetization. Self-demagnetization occurs because the magnetic field from the magnet can pass back through the magnet itself.

All magnets in free space will apply a self –demagnetizing field but only magnets with very low working points and/or low coercive force values will show self-demagnetization.

Rare-earth magnets and Ferrite magnets, in normal operation, do not demagnetize by self-demagnetization. So, this term is not significant for this type of magnet [41].

III. PM MODELLING

A crucial step for a detailed study of ID is the proper definition of the $B-H$ curve of the PM, which describes the demagnetization curve including the knee point. Defining the $B-H$ curve of the PM by conventional B_r and μ_r parameters is not accurate and inapplicable for ID analysis. Therefore, it is necessary to use the developed non-linear model for the $B-H$ curve [11]. The utilized PM models in literature for ID analysis are as follows

A. LINEAR MODEL (LM)

One of the simplest methods to describe the nonlinear behavior of the PM is the linear model. The linear demagnetization models consist of two linear segments, one from the B_r to B_{knee} and the other from B_{knee} to $B = 0$. The linear models could lead to errors due to neglecting the roundness of the knee point. In literature, two linear models of "linear vertical" and "linear sloped" models have been introduced [12]. The general assumptions in implementing the LMs are as follows [15].

1) The details of the main demagnetization loop of the experimental and simulated results are relatively closely matched.

2) the value of $\mu_\Delta = \frac{\Delta B}{\mu_0 \Delta H}$ in partially demagnetized magnet remains equal to μ_r determined at the linear region of the $B-H$ curve. in other words, the slope of the recoil line is the same as the slope of the LM above the knee point.

The mathematical description of the linear sloped model is as Eq. (1).

$$\begin{aligned} B &= B_r + \mu_0 \mu_r H \quad H \geq H_{knee} \\ B &= B_r + \mu_0 H_t (\mu_r - K_0) + \mu_0 K_0 H \quad H < H_{knee} \end{aligned} \tag{1}$$

By fitting the simulated and measured main $B-H$ curves, the values of the presented parameters in Eq. (1) are determined. Also, this equation is capable to present the linear vertical model if the value of K_0 is large enough.

B. EXPONENTIAL MODEL (EM)

As it was mentioned before, the LMs neglect the roundness of the knee point. But using the EM, which is more sophisticated, the roundness of the knee point is considered too. The mathematical expression of the EM is proposed in Eq. (2) [42].

$$B = B_r + \mu_0 \mu_r . H - E . e^{K_1 (K_2 + H)} \tag{2}$$

where μ_0 is the permeability of free space ($4\pi \times 10^{-7}$ H/m), K_1 (sharpness of the knee) and K_2 are the fitting constants, E is a constant for unit conversion, and μ_r is the PM relative permeability. The values of the μ_r and K_2 are calculated using

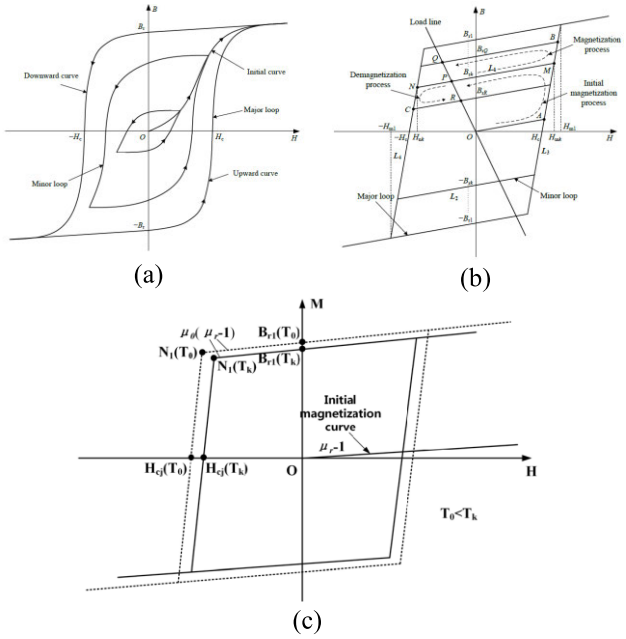

FIGURE 5. (a) Preisach hysteresis model, (b) Linear hysteresis model, and (c) linear temperature-dependent hysteresis model.

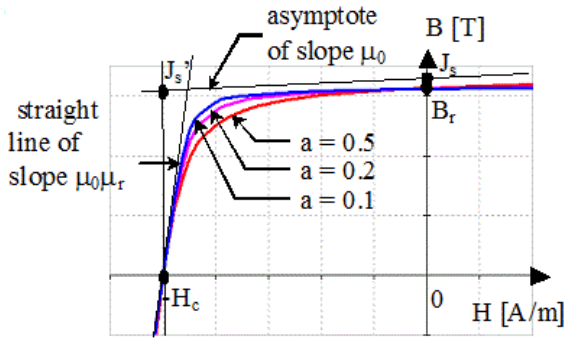

FIGURE 6. The B-H curve model of the PM for FEM analysis (utilized in Flux software) [47].

Eqs. (3) and (4), respectively.

$$\mu_r = \frac{B_r^2}{4.\mu_0.B - H_{max}} \tag{3}$$

$$K_2 = \frac{ln\left[\left(B_r - (\mu_r - 1).\mu_0.H_{jC}\right).\frac{1}{E}\right]}{K_1} - H_{jC} \tag{4}$$

C. HYSTERESIS MODEL

1) PREISACH HYSTERESIS MODEL (PHM)

The hysteresis of ferromagnetic material described by Preisach's theory uses an infinite set of magnetic dipoles which have rectangular hysteresis loops. The combination of the classical Preisach-type model and FEA may lead to some limitations. Also, this model does not account for the dynamic properties of hysteresis nonlinearities [43]. The better choice is the Inverted and forward Preisach models [44] which only

have some vulnerability to the specific B congruency in some regions of the loop. The PHM is shown in Fig. 5(a) and can be expressed as Eq. (5) [45].

$$B = \int_{S^{+(t)}} \cdot \int \mu(\alpha, \beta)\, d\alpha d\beta - \int_{S^{-(t)}} \cdot \int \mu(\alpha, \beta)\, d\alpha d\beta \tag{5}$$

where $S^{+(t)}$ and $S^{-(t)}$ are the positive and negative sets of hysterons of the Preisach triangular region; $\mu(\alpha, \beta)$ is the Preisach distribution function of the dipoles; α and β are the thresholds of the polar reversion of the dipoles with $H_s \geq \alpha \geq \beta \geq -H_s$, and H_s is the saturation magnetic field strength.

2) LINEAR HYSTERESIS MODEL

Compared to PHM which involves multiple integrals, in [46] a Linear Hysteresis Model (LHM) is presented as illustrated in Fig. 5(b). the assumptions of the model are 1. the same value of H_c but with different value of B_r for major hysteresis loop and all the minor hysteresis loops 2. Partly superposes of the major loop by the initial curve

3) TEMPERATURE-DEPENDENT LINEAR HYSTERESIS MODEL

By calculating the temperature coefficient of α, β, and γ, the $M-H$ curve of the PM can be generalized to be temperature dependent as Eqs. (6) to (8) [13].

$$B_{r1} = B_{r1}(T) = B_{r1}(T_0)\,[1 - \alpha(T - T_0)] \tag{6}$$
$$H_{cj} = H_{cj}(T) = H_{cj}(T_0)\,[1 - \beta(T - T_0)] \tag{7}$$
$$H_{N1} = H_{N1}(T) = H_{N1}(T_0)\,[1 - \gamma(T - T_0)] \tag{8}$$

Therefore, using the manufacturing datasheet and calculating the α, β, and γ coefficients, the limiting loop at any temperature T_K ($T_K > T_0$), can be calculated as shown in Fig. 5-(c).

4) KNEE ADJUSTMENT MODEL

In [47] using three parameters of H_c, B_r, and knee adjustment, the non-linear $B-H$ curve of the PM is described. The considered model can be expressed in Eqs. (9) and (10).

$$B(H) = \mu_0 (H + H_c) + \frac{2J_{s'}}{\pi} arctg\left(\frac{\pi(\mu_r - 1)\mu_0 (H + H_c)}{2J_{s'}}\right) \tag{9}$$
$$J_{s'} = J_s + \mu_0 H \tag{10}$$

The description of the parameters is illustrated in Fig. 6.

5) TEMPERATURE-DEPENDENT HYPERBOLIC TANGENT MODEL

The LM and EM can result in considerable errors in ID analysis due to their mathematical structures especially when the operating point of PM falls below H_{cJ} [18]. Therefore, a more developed PM model is required. One of them is the Hyperbolic Tangent Function (HTF) model [48] which can be developed to consider temperature variations. Generally, the temperature effects on the PM model are considered by some temperature coefficient obtained from the supplier's datasheets which are provided by M versus H curve. Therefore, it is better to work directly on $M-H$ curve, instead of $B-H$ curve. Once the temperature dependent $M-H$ curve is derived, it is straightforward to convert $M-H$ characteristic into $B-H$ characteristic. The temperature dependent parameters are B_r and H_{ci}. Both can be described by second order polynomials as Eqs. (11) and (12).

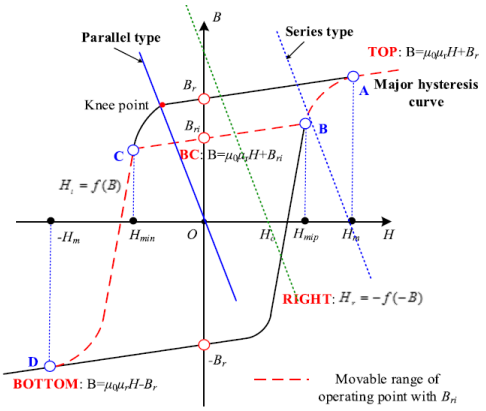

FIGURE 7. Numerical illustration of Fourier series-based hysteresis model [50].

$$B_r(T) = B_r(T_0) \tag{11}$$
$$H_{ci}(T) = H_{ci}(T_0) \tag{12}$$

where, the coefficients of α_1, α_2, β_1, and β_2 are provided in supplier datasheets. Therefore, The $M-H$ curve is described by the HTF as Eq. (13) [49].

$$M(H, T) = P(T)\left(b_0 tanh\left(\frac{H + Q(T) H_{ci}(T_0)}{Q(T) h_0}\right) + b_1 tanh\left(\frac{H + Q(T) H_{ci}(T_0)}{Q(T) h_1}\right)\right) \tag{13}$$

All coefficients of b_0, h_0, b_1 and h_1 can be identified by a nonlinear curve fitting based on the input of a curve at the T_0. Finally, using the terms $P(T)$ and $Q(T)$, the $M-H$ curves at other temperatures are constructed. After that, the $B-H$ curve is simply derived for the second and third quadrants.

Also, the permeability of the recoil line at the temperatures of T_0 and other temperatures are calculated using Eqs. (14) and (15), respectively.

$$\mu(T_0) = \frac{\partial B(H, T_0)}{\partial H}\Big|_{H=0} = \frac{\partial M(H, T_0)}{\partial H}\Big|_{H=0} + \mu_0 = \mu_i(T_0) + \mu_0 \tag{14}$$
$$\mu(T) = \frac{\partial M(H, T)}{\partial H}\Big|_{H=0} + \mu_0 = \frac{P(T)}{Q(T)}\mu_i(T_0) + \mu_0 \tag{15}$$

6) PLAY MODEL

In [14] a TD vector hysteresis model has been presented with the eventual goal of utilizing it in FE simulations. Being

a play-based model, it follows a general approach used in structural hysteresis modelling and is found to have several beneficial features. The computational efficiency is virtually unaffected by the incorporation of temperature dependence, which is included by allowing material parameters such as coercivity and saturation to be functions of temperature. The mathematical expression of the model is as Eqs. (16) and (17).

$$M = \int_0^\infty M_{an}\left(H_{an}\left(\lambda\right), T\right)\xi\left(\lambda\right)d\lambda \tag{16}$$

$$\Delta H_{an}\left(\lambda\right) = \left(1 - min\left(\frac{k\left(T\right)\lambda}{|H - H_{an}|}\right), 1\right) \quad \left(H - H_{an}\left(\lambda\right)\right) \tag{17}$$

where M_{an} and H_{an} are anhysteretic magnetization and inverse function, respectively. λ is a factor scaling, $\zeta(\lambda)$ is a weight function, and $\Delta H_{an}(\lambda)$ is the an hysteretic field for individual hysterons.

7) FOURIER SERIES-BASED HYSTERESIS MODEL

In [50], The hysteresis property of PMs is characterized by a simple Fourier series-based hysteresis model which is suitable for ease of rapid computation. As shown in Fig. 7, this numerical model is utilized to analytically reveal the balanced bidirectional-magnetization. The developed Fourier series-based hysteresis model consists of a set of recoil lines and the major loop. The major loop consists of two branches, and the left one can be represented as a third-order Fourier series expansion.

$$f\left(x\right) = a_0 + \sum_{k=1}^{3}\left(a_k cosk\omega x + b_k sink\omega x\right) \tag{18}$$

where a_0, a_k, and b_k are the Fourier coefficients. The values of coefficients of the Fourier series-based hysteresis model can be obtained by a magnetizer-based experiment.

D. COMPARISON

Generally, PM modelling methods can be categorized into nonlinear and linear. The linear demagnetization model divides the demagnetization curve into two linear segments that intersect at the knee point. On the one hand, linear models have some advantages as low computational cost, simple parameter identification procedure, and reduced risk of numerical problems. Therefore, this method is frequently used in articles [18]. On the other hand, because of the previously mentioned linear assumptions, the error can happen due to neglecting the curve's roundness around the knee point [17]. For the linear sloped and exponential models, due to their mathematical structure, the results may be highly erroneous in case of the operating point of PM falls below intrinsic coercivity [18]. The nonlinear models are more precise, but complex parameter identification procedures, high computational time due to non-linear iteration analysis, high memory required, and the risk of convergence are their main drawbacks [13]. Most non-linear PM models are based on the hysteresis model. To judge the usefulness of the hysteresis model the factors of matching the model with real material properties, acceptable computational time, simplicity of use, and numerical stabilization are important [43]. Among the hysteresis models, in case of reduced squareness of the PM's main B-H curve, the accuracy of the tangent function model may be reduced. To solve this issue, the hyperbolic tangent function model can be used. It uses hyperbolic functions in its structure [48]. Finally, the ability to consider temperature variation is one of the most important factors in the effectiveness of PM modelling techniques.

IV. ID MODELLING

As was mentioned before, one of the critical parts of the PM machine design is the analysis of the ID. For this purpose, an ID modelling method that can realistically simulate the performance of the PM machine during and after the occurrence of the ID is essential. An accurate and efficient ID analysis model will help a designer to select the proper PM material to avoid ID. There are different ID analysis models of the PM machines including FEM [19], Magnetic Equivalent Circuit (MEC) [20], Maxwell's equation [21], Field Reconstruction Model (FRM) [22], Distributed lumped Parameter Model (DLPM) [23], etc. These models have either been implemented directly for ID modelling to investigate the characteristics of the PM machine against external fields or have been used to detect ID faults. According to the purpose of this work, the proposed methods are reviewed in this section as follows

A. NUMERICAL MODELS (FEM)

The FEM is a common and accurate way to evaluate the performance of PM machines. FEM is based on magnetic field analysis, which considers the magnetic circuit, the distribution of stator windings, and the nonlinear behaviour of the ferromagnetic material. The study of the electric field with FEM has the highest accuracy among the modelling methods. Among the various ID analysis models, the FEM has the highest accuracy and has been used interchangeably in various articles. The existing articles in this field are as follows

1) CALCULATING THE ELECTROMAGNETIC CHARACTERISTICS CONSIDERING THE ID

To perform an accurate and systematic ID analysis, the Time Stepping Finite Element Method (TSFEM) should be utilized. In this procedure, the ID is considered at each rotor position and consequently, the accuracy of the results is increased. The modelling flowchart of TSM is shown in Fig. 8. It should be noticed that this procedure is derived from existing papers [19], [51], [52]. Generally, in the literature, this flowchart was utilized for FEM analysis. But with simple modifications, it can be implemented in analytical methods. The process presented in [19] has been implemented with some changes in other articles [53]. This method achieves very high computational accuracy and can model the effect of ID on the output characteristics of the PM machines.

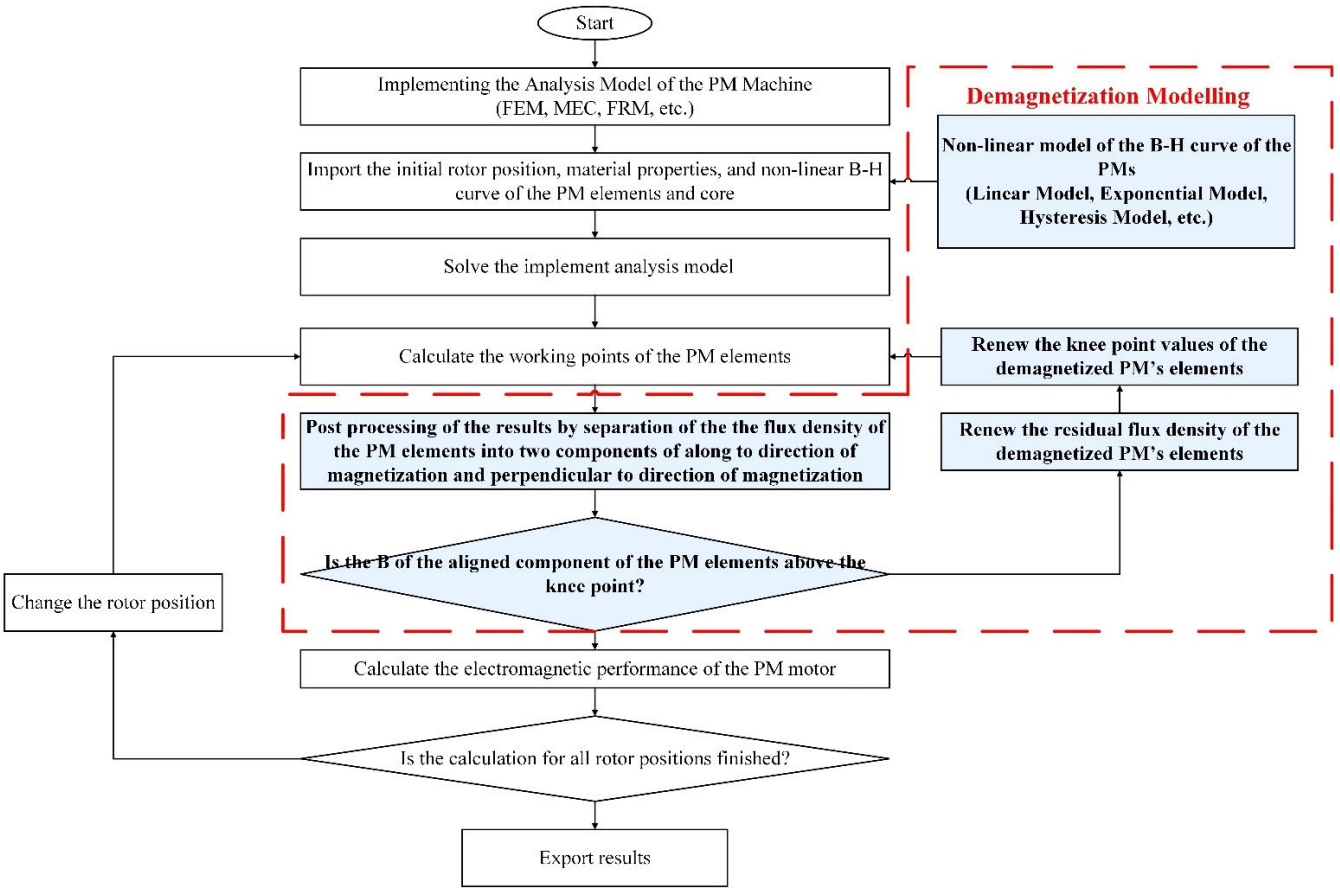

FIGURE 8. Flowchart of TSM.

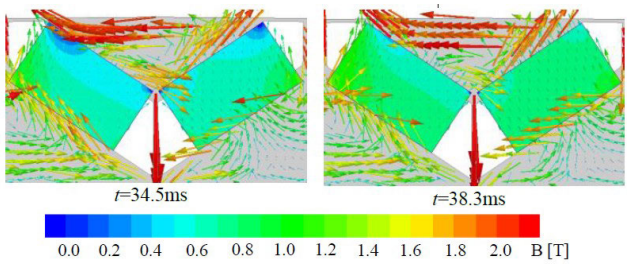

FIGURE 9. Flux density and vector distributions in different time instants [54].

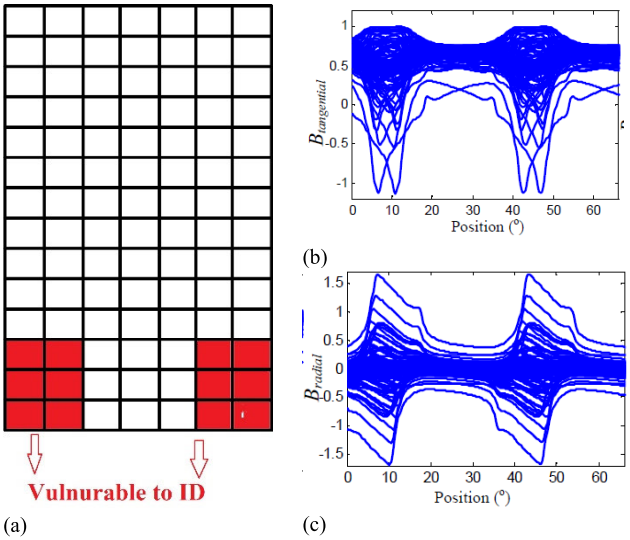

FIGURE 10. Flux density change waveform of each element at one PM versus rotor position (@16 C) (a) PM region drawing (b) tangential component (c) radial component [19].

The presented TSM in Fig. 8 consist of several steps. In the first step it is necessary to accurately implement the analysis model of the PM machine which can be any of conventional analysis model including FEM, MEC, FRM, etc. During implementing the analysis model, it is necessary to use the non-linear B-H model for defining the magnetic characteristics of the PM which based on electric machine design engineer can be any of linear, exponential, hysteresis, etc. The next step is solving the non-linear demagnetization analysis. As it was mentioned before, the criterion for ID analysis is the comparison of magnetic flux density of the working point of the PM's element and the knee point of the B-H curve. The working points of the PM's elements are calculated for each rotor position. The calculated magnetic flux density of the PM's elements should be separated into

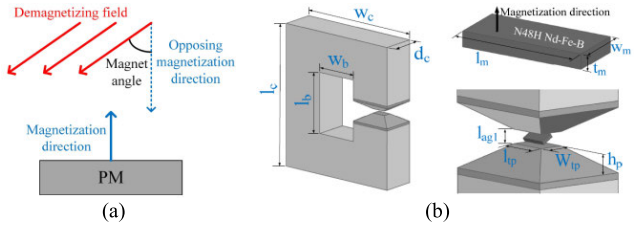

FIGURE 11. (a) Magnet angle definition illustration and (b) a 3D view of the pyramid pole structure [56].

two components of 1. aligned with the PM magnetization direction and 2. perpendicular to the magnetization direction. Because only the aligned component to the magnetization direction should be compared to knee point and this component is corresponded to ID. Therefore, the aligned term will be compared to the knee point value. Two conditions can occur as follows.

1) If the B of the working point of the PM's element was lower than the knee point, the ID has occurred, and the magnet cannot recover its initial B_r. So, it is necessary to modify the amount of B_r in the demagnetized element. Also, the new knee point will be calculated for that element. The non-linear analysis is repeated for that rotor position with new data. Condition one is continued until no ID is detected.
2) If no ID is detected, the non-linear results will be used to calculate the electromagnetic torque of the motor at specified rotor position.

All mentioned quotes and calculations are performed for other rotor positions. Eventually, the electromagnetic torque of the motor for one mechanical period will be obtained.

2) INVESTIGATING THE FLUX PATTERNS AND SPECIFYING THE MORE VULNERABLE REGIONS TO ID

In [54], the symmetrical SC fault currents in the d-q reference are applied to the IPM generator as shown in Fig. 9. FE analysis is used to account for the impact of the ID on the flux field. The results indicate that the corners of the PMs were more vulnerable to ID. In [19], a typical 12/10 flux-switching PM machine is analyzed. The flux density variation waveform of each element at one PM is calculated under open circuit conditions as it was shown in Fig. 10. According to Fig. 10 (a), the PM surface is divided to small regions and the working point of each element is calculated. The flux density in elements that are located near the air gap (highlighted regions in Fig. 10(a)) changes dramatically with rotor position and these regions are more vulnerable to ID.

In [55], the ID characteristic of distributed and fractional-slot winding, an 8-pole, 48-slot, and 6-phase IPM machine was compared. The obtained results indicate that in contrast to Distributed Winding (DW) machines, the Fractional-Slot (FS) has a non-uniform ID for different rotor poles. Besides, the FS machines have higher d and q-axis inductances than the DF machines. Therefore, the lower the SC current in the

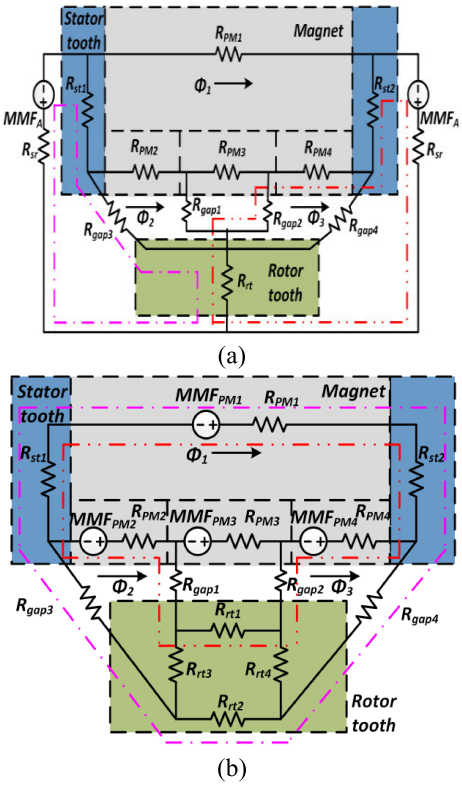

FIGURE 12. The flux path in FSPM motor (a) open-circuit condition and (b) armature winding energized and magnet not magnetized [66].

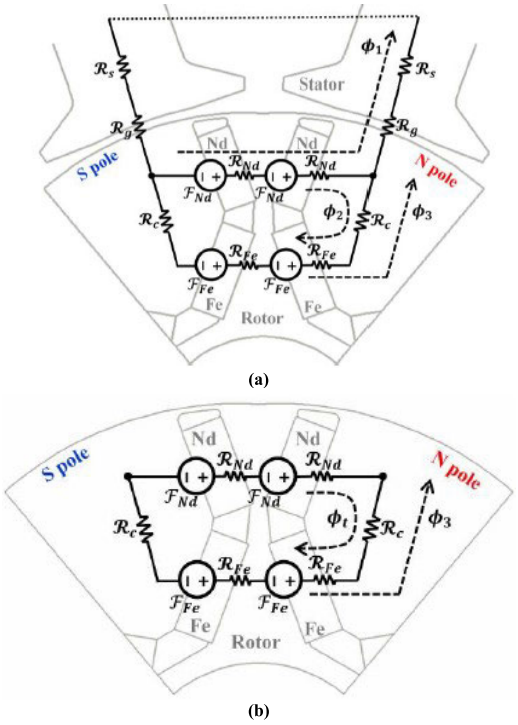

FIGURE 13. The MEC model of hybrid IPM motor (a) with the stator and (b) without stator [67].

FS machine and consequently the lower the ID risk. In some IPM or salient pole machines, the PMs are exposed to DFs

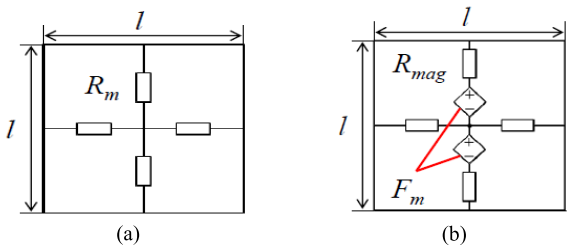

FIGURE 14. Magnetic circuit units (a) core and air (b) PMs [68].

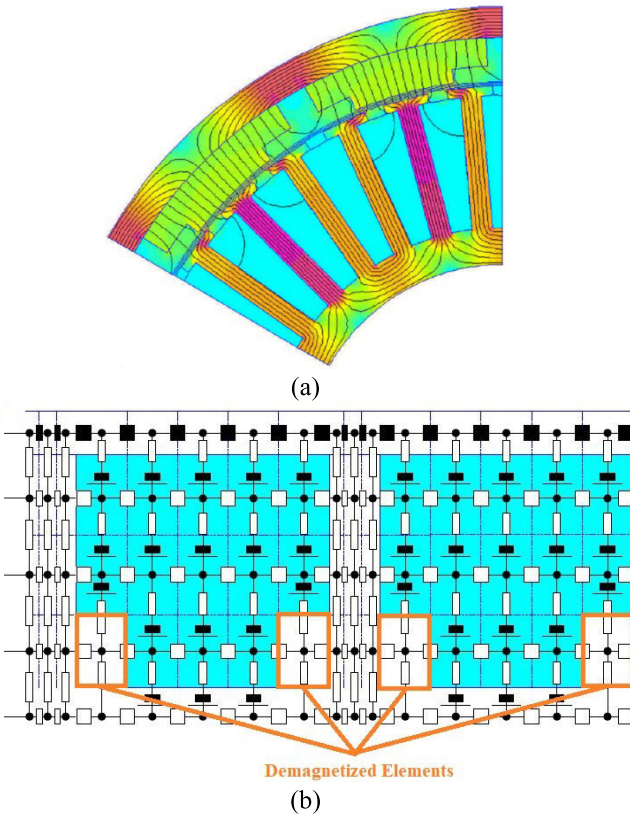

FIGURE 15. (a) The FEM model of the outer rotor SPM motor with symmetric demagnetized area and (b) The MEC model of the SPM motor with 4 demagnetized PM elements [69].

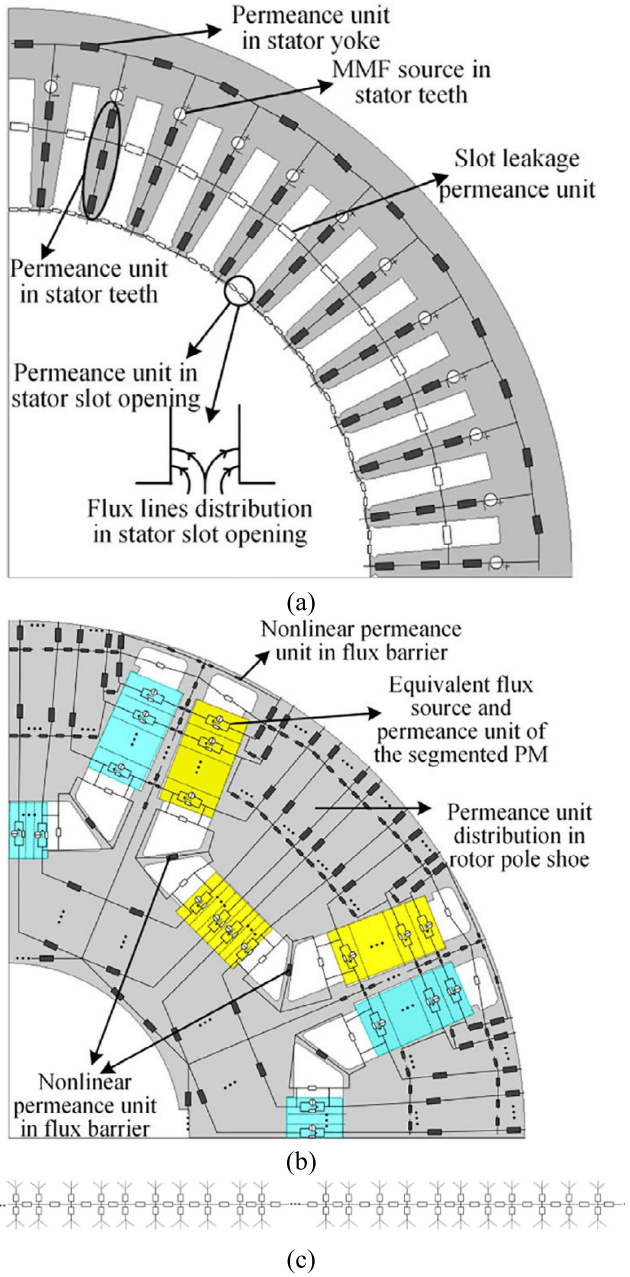

FIGURE 16. The improved MEC model of IPM motor (a) stator, (b) rotor, and (c) air gap [70].

that are often aligned to the axis of magnetization. In [56], the effect of the direction of the external DF on ID has been investigated. The considered structure for FE analysis is shown in Fig. 11. The obtained results indicate that the IDR of the PM increases with a higher external DF in a fixed direction and it is much harder to demagnetize the PM at a higher PM angle.

3) OTHER LITERATURE

In [57] the effect of d and q-axis currents on the ID of IPM machines was investigated. The results state that both d and q-axis current components affect the ID of the IPM machine. Adding a q-axis current increases the ID tolerance. In [58], the effect of lifting torque, dry friction torque, viscous friction torque, speed squared torque, and constant power loads on IDR and SC currents of the SPM motor were investigated. The obtained results indicated that the value of the SC current range of these loads is always lower than the constant speed load conditions. Therefore, to check the ID, only checking the constant speed mode is sufficient and covers other conditions. In [59], the ID characteristics of the Halbach magnetized pulsed alternator were investigated using a linear demagnetization model. The results indicate that the compensating shield leads to an increase in the

TABLE 1. The comparison of analysis models.

No.	Analysis Model	Machine	TYPE	REF	Accuracy	Required Memory	Capability to model partial ID	Computational time	PM Model	TSM
1	FEM	LSPM	2D	[76]	Very high	Very high (100MB -2GB)	YES	Very high (15min to 8 days)	Linear Model	YES
		Memory	2D	[46]					Linear Hysteresis Model	NO
		LSPM	2D	[77]					Linear Model	NO
		IPM	2D	[78]					Linear Model	NO
		SPM	2D	[79]					TD hyperbolic tangent model	NO
2	MEC	PMSM	RN	[69]	High	Low (100KB-10MB)	YES	Medium (20 sec to 4 hours)	Linear Model	NO
		SPM	RNA	[68]			YES		Linear Model	YES
		IPM	MEC	[70]			YES		Linear Model	YES
		RWAFPM	MEC	[47]			NO		Knee adjustment model	YES
3	Maxwell Equations	AFPM	-	[80]	High	Low (650KB)	NO	Low (15 sec)	Linear Model	NO
		PMR		[81]			NO		Linear Model	YES
		Outer Rotor		[82]			YES		Linear Model	NO
		AFPM	-	[74]			NO		Linear Model	NO
		PMSM	-	[75]			YES		Linear Model	NO
		AFPM	CM	[21]			YES		Linear Model	NO
4	FRM	PMSM AFPM	2D 3D	[22] [73]	High	Medium (120MB)	YES	Low (33 sec)	Linear Model	NO
5	DLPM	PMSM	d-q model	[23]	Medium	Low (450KB)	NO	Low (11 sec)	Linear Model	NO

discharge current, and weakens the effect of external DF on the ID.

B. ANALYTICAL MODELS

Although the FEM has the highest accuracy among different modelling methods, in the initial design stage its application is limited due to the high computational time and memory required. In contrast to FEM, the analytical models have less computational time due to the need for fewer parameters and simplifications, such as ignoring the effect of slots and saturation. These models have a compromise between computational time and accuracy [60], [61]. The analytical models to investigate the ID are as follows.

1) MEC MODEL

In recent years, the MEC model has improved and become a popular model for the design and optimization of various types of electric machines, including induction machines [62], linear machines [63], AFPM machines [64], and so on. The MEC model makes a good compromise between computational time and accuracy. This method can consider magnetic saturation, armature reaction, leakage flux, and rotor displacement. The MEC method uses reluctance, which depends on time or position for different parts of the machine to achieve the highest accuracy [65]. In the MEC model, the machine model is divided into many parts, and an equivalent circuit is considered for each part. By connecting all the units of the MEC, the MEC model is obtained. The existing literature for ID analysis by the MEC model is as follows.

a: ANALYZING THE MAGNETIC CIRCUIT TO SPECIFY THE VULNERABLE REGIONS TO ID

In the literature, the MEC model is used to provide conceptual and mechanism explanations rather than detailed quantitative

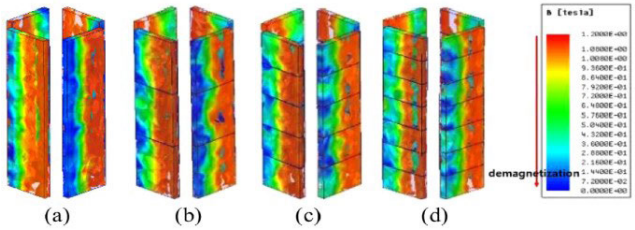

FIGURE 17. Demagnetization characteristics according to magnet division (seven times the rated current) [25].

ID calculations. In [66], the simplified MEC model of the FSPM motor was utilized to specify the vulnerable regions to ID, as shown in Fig. 12. By examining the flux path in different parts of the PMs and air gap, and comparing the permeability of different parts, the vulnerable areas to ID are identified. The results have shown that the left and right corners of the PMs near the air gap were vulnerable to self-demagnetization when the rotor pole was aligned with the magnet. Also, a roadmap to improve the ID tolerance capability was presented. In [67], as it was shown in Fig. 13, the ID analysis for hybrid-type IPM motor was investigated. Using the MEC model, it was illustrated that in case of stator absence, the magnetic field produced by NdFeB can lead to ID in the Ferrite PMs.

b: CALCULATING THE ELECTROMAGNETIC PARAMETERS CONSIDERING ID

Other literature uses the MEC model to calculate the electromagnetic parameters of the PM machines like Back-EMF and torque considering ID. For this purpose, it is necessary to update and calculate the produced MMF of the PMs at each iteration. An example of the MEC units of the core, air gap, and PMs is shown in Fig. 14 [68]. By joining these simple units, the overall MEC model of the PM machines

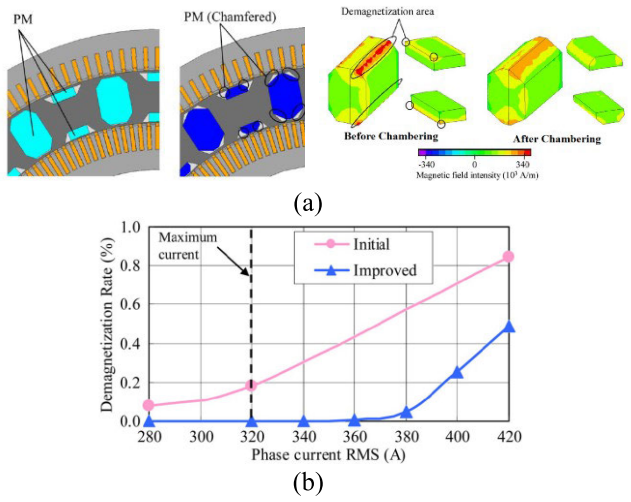

FIGURE 18. (a) Distribution of magnetic field intensity of the initial shape and improved shape (b) IDR characteristics [88].

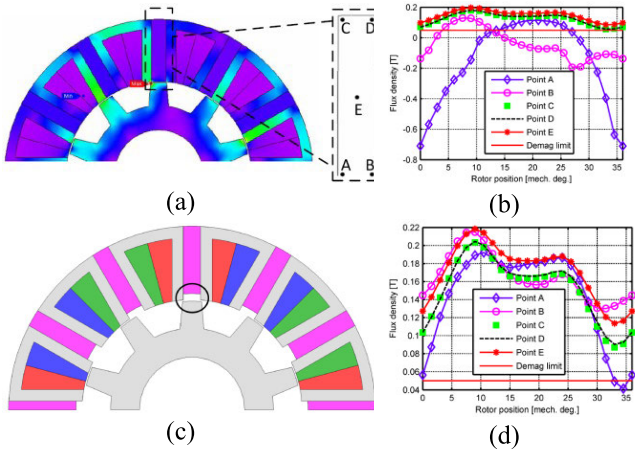

FIGURE 19. (a) Initial FSPM motor, (b) ID condition of the initial design, (c) proposed design with a 2 mm shorter magnet length in radius direction, and (d) ID condition of the proposed design [66].

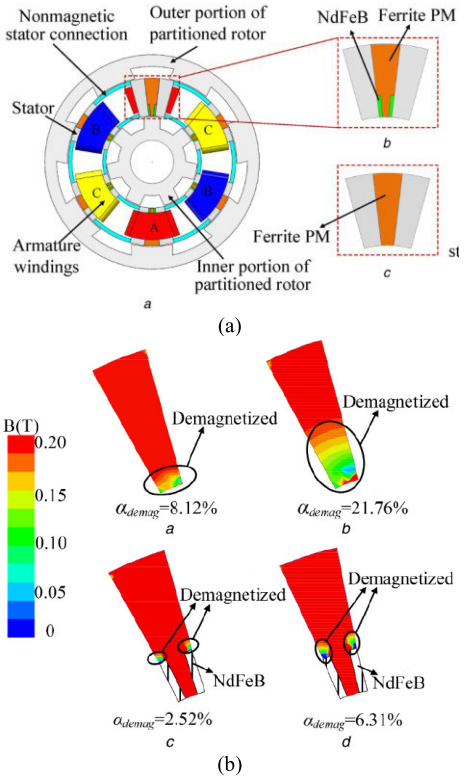

FIGURE 20. (a) The proposed hybrid PM design and (b) the comparison of IDR results [27].

is obtained. In the MEC model, the equivalent MMF of the PM elements is calculated using Eq. (19). In the next step, by solving the MEC of the machine, the working point of the PMs is calculated. Then, the working point of the PMs is compared with the knee point. In the case of ID, the values of the B_r and μ_r for each PM elements must be updated.

$$F_m = F\left(B_r, \mu_r\right) \tag{19}$$

In [69], first, the MEC model of the outer rotor SPM motor is obtained then to modelling the ID, the MMF of the specified PM's elements were eliminated as shown in Fig. 15. The purpose of this work is to establish the modified MEC model to be able to consider ID in optimization and fault diagnosing. Also, the improved model can consider the partial ID.

In [47], using the MEC model, ID modelling of the RWAFPM motor which has a 3D flux path was carried out.

In [70], a more developed MEC model which divides the PMs, air gap, and core parts into small segments was introduced to accurately calculate the working point of the PMs. Also, the proposed model can separate the flux density component along the corresponding magnetizing direction.

Fig. 16 shows the developed MEC model and its structural details. The purpose of this paper is to propose a simple MEC calculation to calculate the IDR of the 3D flux path PM machines in the initial design stage with acceptable accuracy. The results have shown that the computation time of the MEC model compared to the FEM model was reduced from 3 hours to 35 seconds.

In addition, some articles use the MEC model to give design and operation consideration to avoid ID. In [71], the maximum allowable current level in the PM-shield ADS-SRMs at various PM temperatures was calculated to avoid ID for the rare-earth and ferrite PMs. In [72], the design considerations and sensitivity analyses of the LSPM motor to improve the ID withstand capability have been carried out.

2) OTHER ANALYTICAL MODELS

Although the FEM and MEC are the two most favourable modelling method for ID analysis, there are some ID modelling methods which is presented in literature including Maxwell's Equation FRM, and DLPM. These methods are

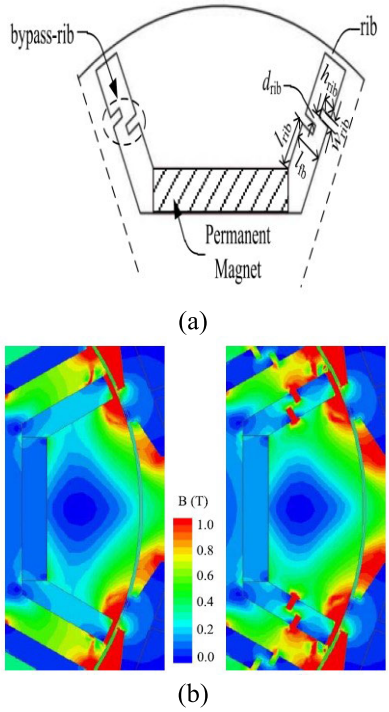

FIGURE 21. (a) The modifications in the rotor design, and (b) the improvement made in magnet flux density [28].

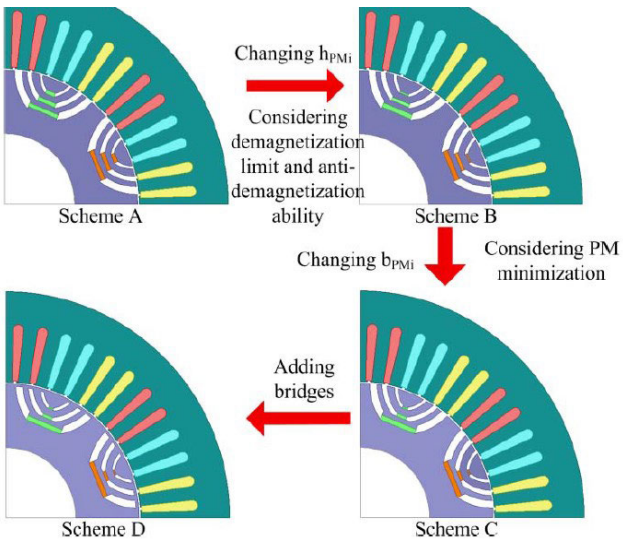

FIGURE 22. The modifications of the LRE-IPMSM motor structure [90].

not mature yet but because of their low computational time and acceptable accuracy attract some attention. Reluctance network and FRM-based models only model one slot therefore, they are faster than the FEM model [73]. Another analytical method is to solve Laplace equations. In this method, the analytical model can be obtained by directly solving Maxwell magnetic equations. In this method, the magnet is divided into different parts and the equations of air distance potential vectors for each part are obtained and solved. The total potential

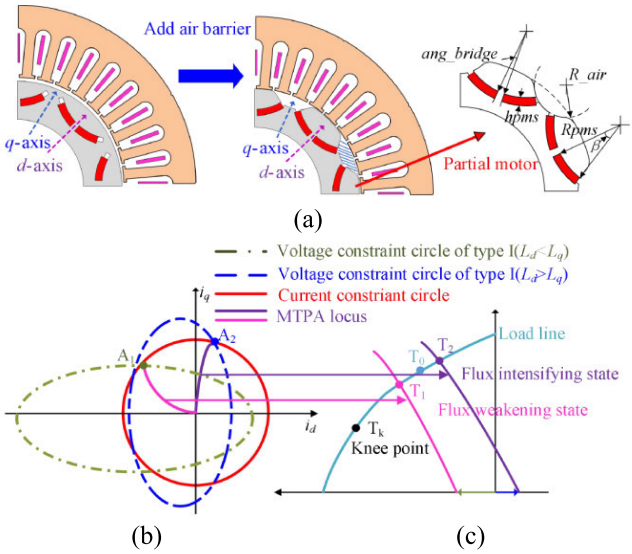

FIGURE 23. The changes reverse the saliency ratio and the relationships between different inductance characteristics and PM operation points (a) applied geometry modifications (b) Current voltage constrain circles. (c) PM operating points at different operation states [91].

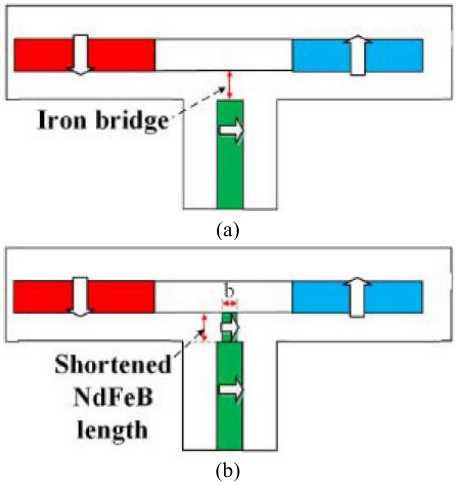

FIGURE 24. (a) The initial structure and (b) the modified design [92].

of the air gap potential is obtained by summing the values obtained above. Therefore, PM localization is modelled by placing air gaps in place of some sections or reducing the density of the residual flux in these areas [74], [75].

C. COMPARISON OF ID ANALYSIS MODELS

Different analysis models of the ID are compared in Table-1 in terms of machine type, accuracy, required memory, capability to model the partial ID, computational time, PM model, and TSM.

V. OPTIMIZATION

The essential step in the design of the PM motor is geometry optimization to achieve the desired output responses. In most cases to avoid high computational time and memory

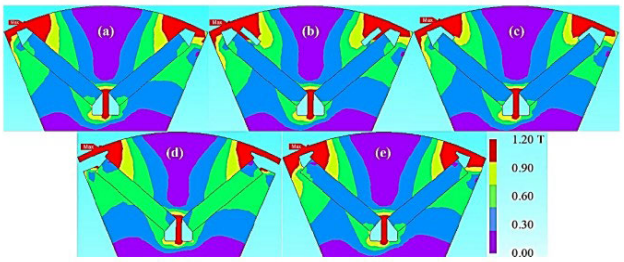

FIGURE 25. Distribution of flux density in the rotor with different rotor flux barriers arrangements [5].

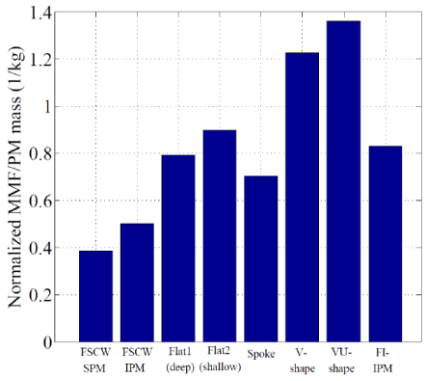

FIGURE 26. The calculated ID indexes [95].

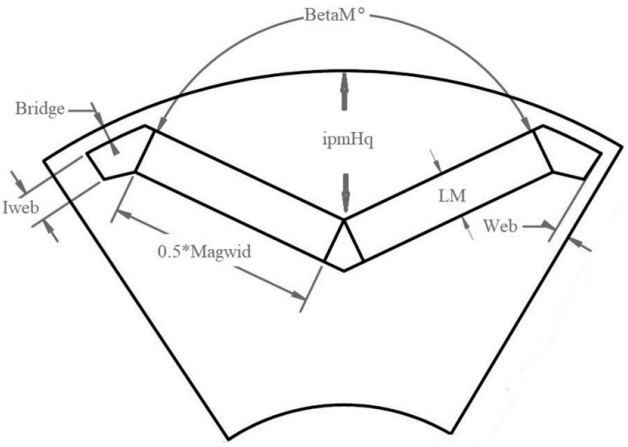

FIGURE 27. The design parameters of the IPM motor [1].

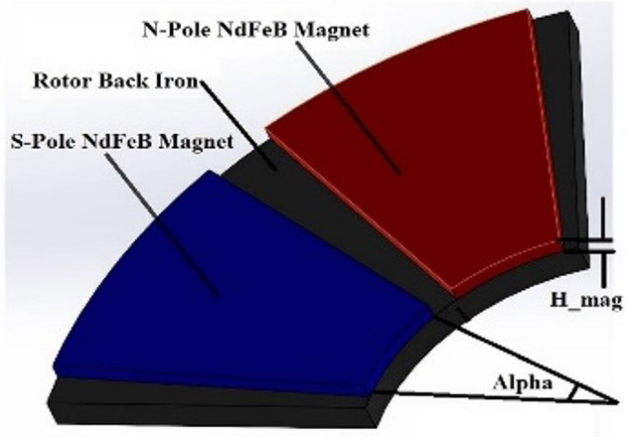

FIGURE 28. The rotor parameters of ring winding AFPM motor [97].

required, due to non-linear and high dimensional nature of the geometry optimization, the indirect methods based on Design of Experiment (DOE), approximating model, or a combination of these two methods are utilized [83]. The DOE based method can efficiently be implemented by Orthogonal Array (OA) and Taguchi Method. For example, in [84], system-level design optimization method for a permanent magnet hub motor based on the actual operating environment is proposed. The Kriging Model (KM) is considered as approximating model and NSGA-II as the optimization algorithm. In [85], A Fuzzy-based sequential Taguchi robust optimization method is utilized to improve the fault-tolerant capability of the PM hub motor which results in efficient comprehensive performance and saves computing time. In [86], a multi-level multi-objective optimization algorithm is implemented using a combination of the sequential Taguchi method, KM approximating model, and NSGA-III algorithm, which greatly shorten optimization time.

As it was mentioned before, different kinds of output responses can be considered in the optimization procedure. One of the considered output responses in design optimization process is the ID fault-tolerant capability of the PM machines which will be examined in following section in details. Existing articles on improving the performance of PM motors against ID can be categorized as follows

A. REDUCING THE EDDY CURRENT LOSS OF THE PMs

The technical literature on this subject generally focuses on temperature improvement of PMs by reducing eddy current losses. Eddy's current losses increase the temperature of the PM and in consequence increase the risk of ID. In [87], with 3D modelling of eddy current losses, it was found that the major part of eddy current losses is related to inverter carrier harmonics. In [24] and [25] it was shown that by dividing the PMs, the eddy current losses could be reduced and the probability of ID has been reduced. The effect of PM dividing on ID is illustrated in Fig. 17.

B. REMOVE OR REPLACE THE DEMAGNETIZED AREA

One of the proposed methods for reducing the IDR of the PM machines is removing the portions of the PMs which is vulnerable to ID or replacing those areas with stronger PMs. For example, in [88], the FEM results show that the corners of the utilized PMs in PMa-SynRM are exposed to high external DF and vulnerable to ID. Therefore, these regions were chambered to reduce the IDR as shown in Fig. 18 (a). Chambering the corners results in a large magnetic resistance gap between the rotor core and the magnet, which makes it difficult for any demagnetizing field to be applied. The ID

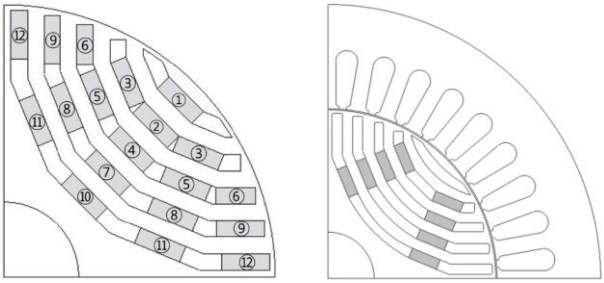

FIGURE 29. (a) The possible PM positions, (b) the optimum design [29].

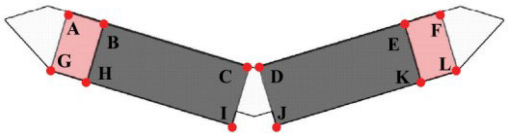

FIGURE 30. The considered points for ID analysis [6].

characteristics of the initial and improved design at different levels of the applied current are shown in Fig. 18 (b). The results indicate that for the improved design, in contrast to initial design, at maximum current there is no risk of ID. Also, the improved design present better ID tolerant capability for higher currents compare to initial design and it confirmed that the improved shape significantly reduces the ID rate, and the PMs are not demagnetized even at maximum current.

In [66] and [89] the exposed regions to high external DF of the FSPM motor were specified. The results show that the regions near the airgap are the most vulnerable regions to ID as it was shown in Fig. 19 (a) and (b). In [66] to reduce the risk of ID a novel design with a 2 mm shorter magnet length in the radius direction was proposed. the ID characteristics of the proposed design are illustrated in Figs. 19 (c) and (d). In [26], with PM shaping the vulnerable region to ID is removed to decrease the IDR. Theoretically, removing the useless portions of the PM which were not contribute to torque production is useful and it reduces the mass and cost of the PM. But in practice, this can lead to a small reduction of produced torque. Another technique is replacing the demagnetized area with stronger PMs to reduce the risk of ID. In [27], the idea of using hybrid PMs for a specific topology of the ferrite FSPM structure was presented. The authors suggested replacing the PMs in areas exposed to high DF with NdFeB PMs. The corners of the Fe-PMs were replaced by a NdFeB magnet. To check the efficiency of the modifications, by applying a three-phase SC current, the IDR and variation of the magnetic flux density of the PM's working point have been investigated. These results are shown in Fig. 20. The obtained results indicate that this improvement in the design has led to a decrease in the IDR.

C. OPTIMIZING THE STRUCTURE OF THE MAGNETIC CIRCUIT TO PROTECT THE PMs AGAINST EXTERNAL DF

Researchers have done a lot of research to solve the problem of ID in PM machines. Their efforts include optimizing the structure of the magnetic circuit, reducing losses, using barriers to change the direction of flux, and the influence of various design factors to reduce the possibility of ID. In [28], the ID condition of the PMa-synRM motor is improved using bypass-rib. The modification and its effect on ID are shown in Fig. 21. In [90], the effect of various parameters such as magnet width and magnet thickness on improving the ID condition LRE-IPMSM motor was investigated. The obtained results indicate that the thickness of the magnet is more important than the width of the magnet. The process of geometry modifications is illustrated in Fig. 22.

In [91], the idea of a reverse saliency ratio ($L_d > L_q$) was used to improve the field weakening conditions of PM motors, which will lead to an improvement in the ID condition. The applied changes to provide the condition of $L_d > L_q$ is shown in Fig. 23 (a). On the one hand, by widening the intermediate bridge between two magnets, the magnetic reluctance of the d-axis increases. On the other hand, adding a flux buffer in the air gap of the q-axis increases the reactance of this axis. By that way, the saliency ratio was changed. Fig. 23 (b) shows the current and voltage constraint circles of two inductance characteristics with MTPA control for the motors with $L_d < L_q$ and $L_d > L_q$ which operate in flux-weakening state by negative and positive d-axis current, respectively. The corresponding PM operation points are showed in Fig. 23 (c). When motor operates under positive d-axis current, the PM operation point would move from T_0 to T_2 which results in lower risk of ID.

In [92], as it was shown in Fig. 24, by inserting small amount of NdFeB PMs into the iron bridge, the working point of the PM moves higher, and the ID withstand capability of SF-HMMM is improved. In [5], different combination of the flux barriers in V-shaped IPM motor are compared. As shown in Fig. 25, with placing the flux barriers on the q-axis of the rotor (model D), it mitigates the impact of armature current and current phase advance on the distribution of PM flux on the q-axis. This helps PMs avoid being demagnetized and reduce saturation on the stator teeth.

D. PROPOSING THE DESIGN TIPS OR COMPARING DIFFERENT TOPOLOGIES

In [54], the influence of slot-pole combinations and rotor types on the ID of the 7MW IPM generator with FSCWs was analysed. The paper concludes that the larger slot per phase per pole and double-layer windings can effectively improve the anti-demagnetization capacity of large-scale IPM generators with FSCWs. In [93], ID characteristics of the IPM and SPM motors have been investigated. The results showed that the IPM motor has a higher ID tolerance than the SPM motor. In [94], three IPM motor models with different magnet structures including single-layer, V-shaped, and double-layer were

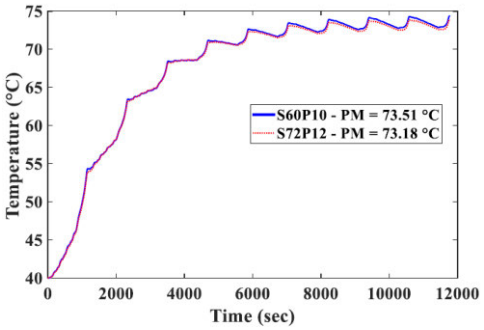

FIGURE 31. Transient temperature of IPM motor under 10 driving cycles of NEDC [1].

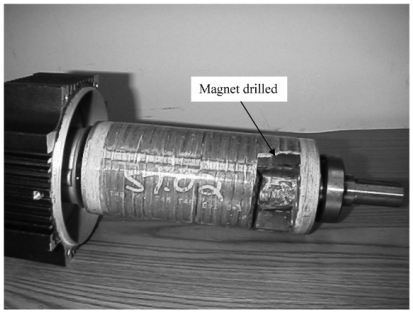

FIGURE 32. Photo of rotor with a section of the magnet material removed.

examined in terms of ID. It was found that the single-layer model has the highest probability of ID under the conditions of maximum torque. Model V is also the most vulnerable in terms of ID under SC conditions. Finally, it was found that the double-layer model has the highest tolerance against ID. In [95], eight topologies of PM synchronous machines were compared in terms of ID. In this paper, to rank the different topologies, a new ID index was introduced which considers the mass of the utilized PMs. The ID index is expressed as Eq. (20).

$$ID\ index = \frac{Normalizeddemagnetization MMF}{PMmass} \tag{20}$$

The calculated ID indexes for eight topologies are illustrated in Fig. 26.

In [96], series of low-cost AFPMSMs with hybrid NdFeB-Ferrite magnet materials with parallel and vertical magnetization patterns are compared in term of ID fault tolerant capabilities. Also, the ID ratio defined as Eq. (21).

$$IDR = \frac{E_1 - E_2}{E_1} \tag{21}$$

where E1 and E2 are the RMS values of the terminal voltage in the phase before and after applying the demagnetization current and temperature condition, respectively.

E. INVESTIGATE THE PARAMETERS VARIATION

In [1], The effect of the rotor geometry parameters on the IDR of the IPM motor is investigated. Magnet angle and air gap length are two factors that directly affect the percentage

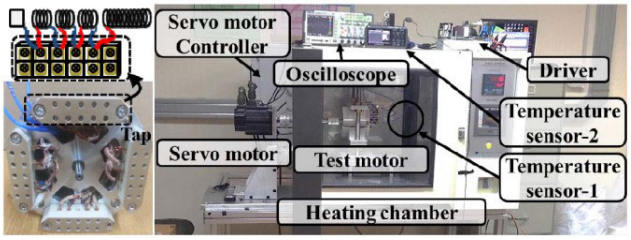

FIGURE 33. Experimental setup for ID analysis [53].

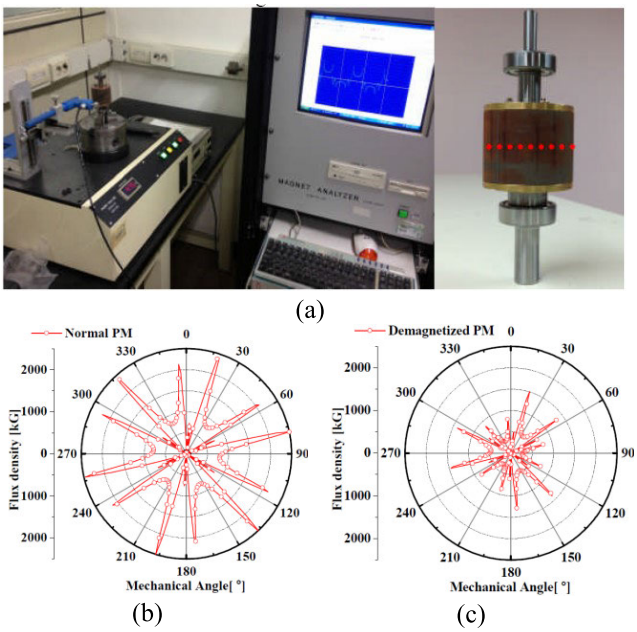

FIGURE 34. The surface magnetic flux density of rotor (a) Equipment for measuring surface magnetic flux density (a) normal PM and (b) demagnetized PM [105].

of ID. Any increase in these two factors causes the IDR to increase under nominal current at the greatest temperature. While lengthening the air gap can decrease IDR, it has a negative effect for the power factor, back-EMF, and average torque. The iron bridge offers an extra route for PM flux leakage. The linkage flux of the PM decreases as the bridge length increases. More DF will travel through the PM and further the IDR. Since a thinner bridge is fully saturated and unable to pass any more flux. There are no significant effects of the Iweb parameter on IDR. The corners of the magnet move closer to the air gap as the magwid increases, exposing them to stronger DFs and raising the risk of ID in those regions. The PMs field at the intersection of the PMs of the one pole increases as the Betam increases, decreasing the air pocket length at the corner of the PMs and decreasing the ID risk. The PM is further buried inside the rotor core as the Ipmhq rises, and the IDR decreases. The higher Ipmhq at the constant magnetization direction also results in a greater angle between the DF and PM magnetization directions, which lowers the risk of IDR. The higher the *LM* produces the higher MMF so the required external field to ID will be

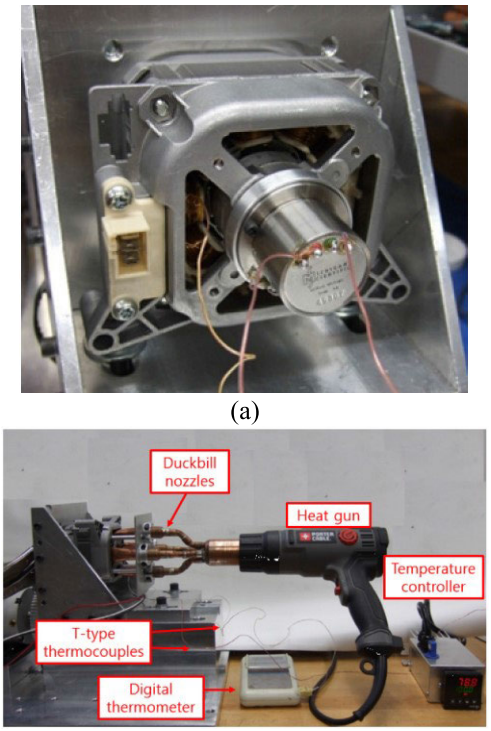

FIGURE 35. (a) The motor under study (b) Heat gun and the heat transfer paths created to increase the temperature of the rotor [95].

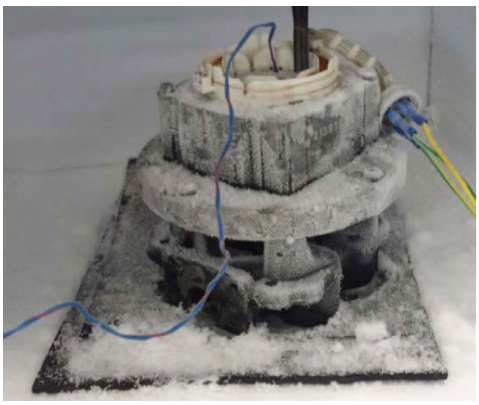

FIGURE 36. BLDC 6/4 motor in a refrigerator for demagnetization tests at −20°C [106].

increased. In other words, the thicker PM increases the load line slope of the motor as a result, the higher working point and lower ID risk. In addition, because the thicker PM has a lower viscosity coefficient, the rate of magnetization loss will be slower over time. The air pocket length decreases as the web length increases. As a result, the IDR will be lower.

The impact of rotor parameters on the ID of ring winding AFPM machines was researched in [97]. Fig. 28 depicts the parameters that were studied. The findings show that the IDR is significantly reduced as the magnet thickness increases, and this parameter's effectiveness is greater than that of other factors. The thicker PM creates higher MMF and causes the

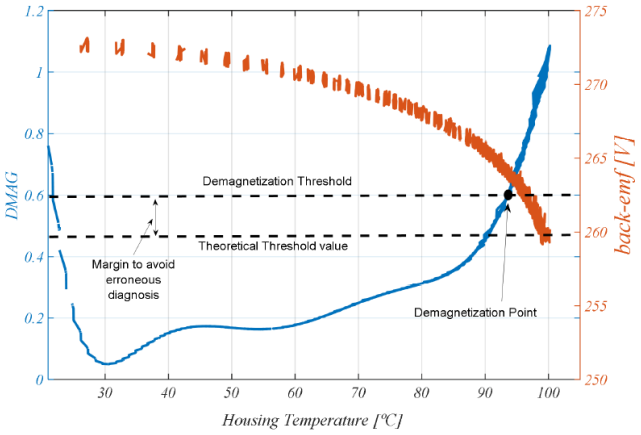

FIGURE 37. ID criteria corresponding to DMAG values [107].

motor's load line slope to increase. It results in a higher working point and consequently a lower risk of ID. Moreover, a lower viscosity coefficient will result in a slower rate of demagnetization loss over time. Also, magnet angle and air gap length are two factors that directly affect the percentage of ID. Any increase in these two factors causes the IDR to increase under nominal current at the greatest temperature.

F. CONSIDERING THE ID IN THE INTELLIGENT DESIGN OPTIMIZATION PROCESS

So far, little effort has been made to consider the ID phenomenon in the design process of PM machines. Most of the papers evaluate the ID after the optimization procedure [98], [99]. For example, in [100] and [101], after performing the optimization procedure to compare initial design's and modified design's ID characteristics, the post-processing ID analysis was carried out.

However, some new articles consider ID in the design process. In [29], the optimum position and combination of the PMs to achieve the required performances were specified. In the design process for each possible solution, the ID is checked as a penalty function. The results show that the models with the magnets located at the side (No. 3, 5, 6, 8, 9, 11, 12) are more vulnerable to ID than those with the PMs located at the centre. The possible PMs position and the combination of the modified design are illustrated in Fig. 29.

In [6], first by considering 12 points along the PMs in the IPM motor and using FEM analysis, it is found that the corner of the PMs (point A in Fig. 30) is the most vulnerable region to ID. In the next step, the significant parameters for improving the flux density of point A were specified which were span angle and pole length. Thus, they are taken as the variables. To avoid the ID, it is necessary to check Eq. (22) for each optimization iteration as a penalty function. When magnetic pole geometries satisfy Eq. (22), it is considered that the ID check meets the requirement.

$$Length + 0.22541 \times SpanAngle - 50.4918 > 0 \qquad (22)$$

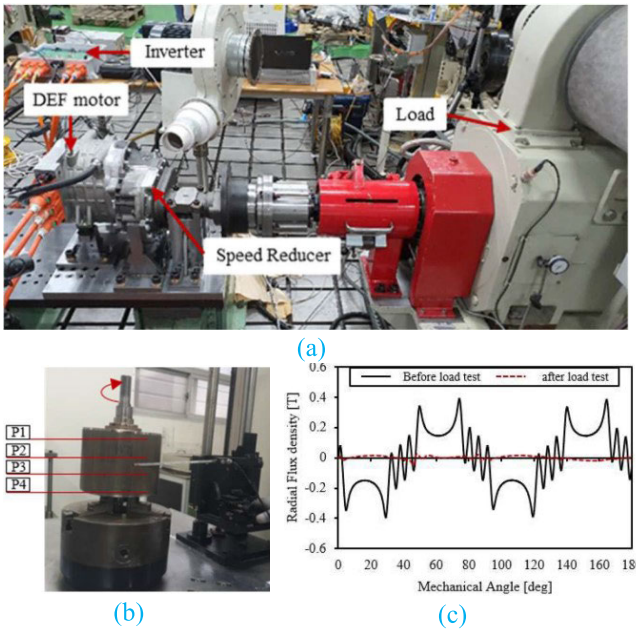

FIGURE 38. (a) Experimental setup with DEF motor (b) Measurement points on the rotor, (c) Measurement results of radial flux density on point P3 [108].

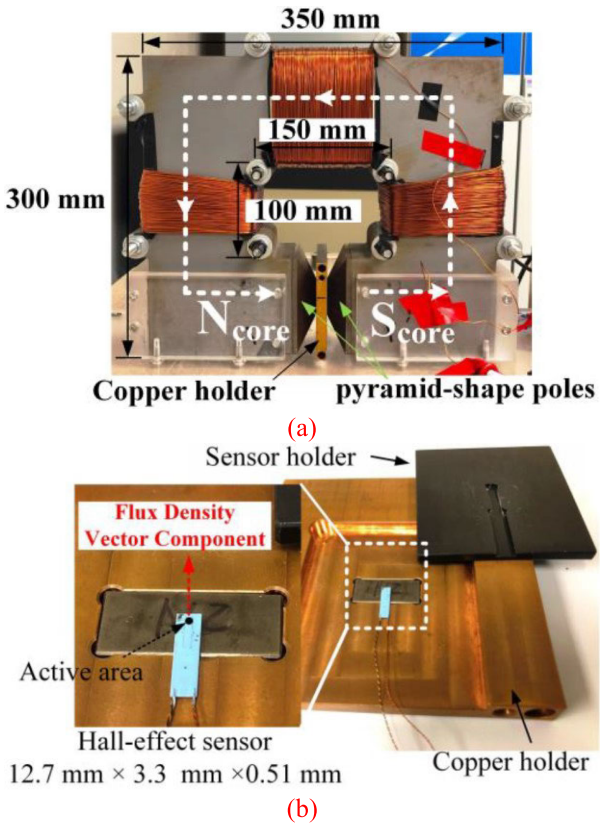

FIGURE 39. (a) Demagnetization test fixture, (b) the location of the hall-effect sensor regarding PM location [109].

In [1] first, the design tips to reduce the probability of ID of the IPM motor for electric vehicle applications were presented. Then, the fault-tolerant design in the case of ID is carried out using the two-level Taguchi optimization approach. In this paper, the ID is considered as one of the objective functions (T_{ave}, T_{rip}, V_{PM}, $andIDR$). To calculate the IDR, for each design combinations, using image processing software the area of the ID regions was calculated. Then, using Eq. (23) the IDR is calculated.

$$IDR = \frac{DemagnetizedArea}{OverallAreaofthePM} \tag{23}$$

In [102], the optimal design process of spoke type IPM motor allowing a limited amount of ID was presented. The primary purpose of optimal design, which allows up to 3% ID of PM, was to minimize PM usage while satisfying motor performance requirements such as efficiency, output power, etc. In this paper, the IDR is considered one of the objective functions. To calculate the IDR, the amount of change in the motor torque constant [Nm/Arms] in the i-th analysis before and after the ID analysis is expressed as Eq. (24).

$$IDR\,(i) = \frac{K_{T_{after}}\,(i)}{K_{T_{before}}\,(i)} \times 100 \tag{24}$$

The optimization results indicate that compared to the initial design only 3% IDR occurred while the weight of the PM is significantly reduced by 23.7%. In [103], a novel fault-tolerant design process of a spoke type IPM motor is presented. to compensate for the degraded motor torque constant caused by degraded PM. In the design process, ID characteristics of each design is calculated and based on the target torque constant, required by the integrated electric brake system a compensation coefficient is introduced to increase the stacking length. The proposed method results in the possibility to significantly reduce the motor volume by 12.9% compared to the conventional optimized model in which ID was not allowed at all.

VI. EXPERIMENTAL ANALYSIS

So far, little attempt has been made to model the ID in practice, due to the destructive nature of ID experimental analysis. The ID is depended on the working temperature of the PM. To accurately measure the ID in the experimental setup, the following topics should be considered.

1. Most of the electric machines are designed for conventional industrial application which have a specified load. For this type of the PM machines the PM will reach it steady state temperature after the specific time period. Therefore, for this type of PM machines, the ID should be measured after they reach their steady state condition. At this condition the motor is un-loaded, and the open circuit voltage of the motor is measured and compared to the initial measured open circuit voltage. The difference between these two open circuit voltages will be known as ID.
2. For the PM machines utilized in EV applications, the PM machines experienced different load condition and they must work under different driving cycles. For this

type of machine, it should be considered that the temperature rise constant of the electrical machines is high. So, the working temperature variation does not occur in the limited over-load or acceleration period. For example, the variation of the PM temperature of the designed IPM motor in an EV application over ten driving cycles of NEDC is illustrated in Fig. 31 [1]. The results indicate that the overall temperature of the motor experience a little variation in the specific driving cycle operation. Therefore, for this type of PM machines, the ID should be measured after working for 5 to 6 driving cycles and comparing the open circuit voltage results to specify the ID.

In the previous studies, in most cases, a part of PM was removed to investigate the effect of ID, as shown in Fig. 32, using a drill or other device [104]. Then by analyzing the PM machine's signals, the ID fault and its severity are detected [3], [30], [31]. The drawback of this method is that ID generally occurs partially in all PMs, not in a specific PM. Therefore, this method does not present the real conditions of ID.

The second method is based on heating the motor and injecting high-amplitude currents or SC conditions to create ID conditions [32], [33]. These methods present the real ID conditions compared to the first method. In these methods, by comparison of Back-EMF [53] or surface magnetic flux density of the rotor [105] before and after the experimental test, the ID is investigated. To heat, the PMs different experimental setups are utilized including a chamber, heat gun, etc. In [53], the test bench is implemented according to Fig. 33. The heating chamber heats the motor to match the operating temperature of the PM. Temperature sensors 1 and 2 are used to estimate the surrounding temperature of the motor and the PM temperature. The temperature inside the motor increases with delay, so it is necessary to place the sensor inside the motor to measure the test temperature properly. Temperature sensor-1 measures the outside temperature of the motor, and temperature sensor-2 measures the inside temperature. The servo motor and its controller are used for loading the test motor at the rated load and rotating the test motor to measure the back EMF. An inverter is installed to limit the current at 30 A to protect the driver circuit from high fault currents. The inside part of the motor is heated sufficiently by the chamber to 150 °C. To create the SC current, the winding tap is considered for the motor. With increasing the number of faulty turns, the ID fault-tolerant capability of the BLDC motor was investigated. By comparison to Back-EMF, the occurrence of ID was validated.

To compare the surface magnetic flux density of the rotor in [105], the same experimental setup is utilized. Using a magnet analyzer, a path line is considered surrounding the rotor and the magnetic flux density before and after the ID test is obtained, as shown in Fig. 34.

Unlike the previous reference, in [95], as shown in Fig. 35, only the rotor and the PMs were heated, and the temperature of the rotor was increased in a controlled way using a heat gun. Several thermocouples were used to measure the temperature of the rotor, on the rotor. They transmit the measured signals using slip rings. Using this test bench, several ID experiments were performed at different temperatures, and the results were compared with the results obtained from the FEM model.

Previous mentioned experimental test setup was implemented for NdFeB magnet. Therefore, to investigate the ID it as necessary to heat the rotor and PMs. But, in [106], The experimental tests have been performed in a Ferrite BLDC motor and test temperature has been controlled at −20°C to be consistent with the PM curve used in the ID analysis. Fig. 36 shows the motor inside the refrigerator used to control the temperature. A DC voltage source is used to apply DC currents into the stator windings. Then the ID of the Ferrite BLDC motor is investigated by comparison of Back-EMF value before and after injecting current.

The previous experimental test setups are complex and require additional sensors and devices. Therefore, they are not practical in industrial environments. Also, in all cases, the intensity of the ID was not controllable, and they could not identify the exact moment at which the ID occurs. Therefore, in [107], a simple method was proposed for the online estimation of ID to overcome these issues. The requirements of the proposed method include a low-cost thermocouple placed in the housing of the machine and knowledge about the properties of the PMs. The back-emf expression accounting for the working temperature of the PMs and ID can be defined as Eq. (25) [107].

$$E_n = E_{(n-1)} \frac{M_n}{M_{n-1}} \left(1 - \frac{\alpha_m}{100} \left(T_{m(n)} - T_{m(n-1)}\right)\right) \quad (25)$$

where T_m is the temperature of the PM, E is the measured Back-EMF, $\alpha_m \left[\frac{\%}{^\circ}C\right]$ is the thermal coefficient of the PMs, M is the magnetization level, and the subscript 'n' is the sampling instant. A well-known standard procedure for decoupling the influence of the temperature is checking the back-EMF at room temperature, before and after the ID test. However, this method is not valid for an online evaluation ID. Based on Eq. (25), knowing the PM temperature, these two parameters can be decoupled. In most PM machine topologies, the PMs are in the rotor. Therefore, it is difficult to measure the PM temperature directly. In [107], to avoid using the temperature sensors for PMS, the relation between the housing temperature and the Back-EMF is derived in real-time. Therefore, the ID severity factor (DMAG) is calculated based on Eq. (26).

$$DMAG = \frac{E_{(n-1)}\alpha_m}{100} + \frac{E_{(n-1)}\left(1 - \Delta M_{(n)}\right)}{T_{h(n)} - T_{h(n-1)}} \quad (26)$$

where T_h is the temperature of the housing. The variation of DMAG versus the housing temperature and ID criteria corresponding to DMAG values for a typical PM machine is illustrated in Fig. 37.

In [108], the effect of Dynamic Eccentricity Fault (DEF) on ID characteristics of IPMSM motor is experimentally

investigated. The results show that in the case of DEF, since the length of the air gap is not constant, the magnetic flux density distribution is distorted, and iron loss is increased. As the iron loss increases, the temperature rises, and an ID fault of the PM occurs due to overheating. The test setup is composed of an electric-axle structure in which the DEF motor and the speed reducer are assembled as shown in Fig. 38. The motor was under test for 114 minutes with working condition of the average torque of 475.1 Nm and the speed of 8700 RPM. After experimental test it found that the BEMF of the motor is significantly decreased. To analyze the cause of this problem, As shown in Fig. 38 (b), the radial flux density the radial flux density of the rotor was measured using a gauss meter. After the load test, since IDF occurred, the radial flux density decreased at all points P1 - P4. Figure 38 (c) shows that the radial flux density decreased by 93.2%. Since point P3 lies at the central region of the rotor along the axial direction where the heat concentrates, the radial flux density decreased more at this point than at the other locations due to DEF.

Also, the technical literature contains some articles about ID investigation on the PM samples alone. In [109], an ID test setup and a DC power supply were utilized to apply a controllable DF current to PM samples used for EVs and their time-dependent demagnetization behaviour was investigated, as shown in Fig. 39. For online measurement of the magnetic field under a constant DF over a wide time range, a Hall-effect sensor was used. In addition, the buck-converter was used to generate a pulsed DF in the timescale of milliseconds. The results indicate that the flux density distribution of PMs demagnetized by a pulsed field is initially highly inhomogeneous. However, applying multiple DF pulses, it tends to become homogeneous.

VII. SUGGESTIONS

Regarding the design optimization of PM machines, to avoid ID some design tips can be suggested. Generally, in PM machines, the produced DF by the windings is passed through the air gap and core to reach the PMs. Therefore, the design considerations are as follows:

A. USE THICKER PMs

The higher the PM thickness the higher MMF. So, the required external field to ID will be increased. In other words, the thicker PM increases the load line slope of the motor as a result, the higher the working point and the lower the ID risk. The thicker PM has a lower viscosity coefficient, so the magnetization loss over time will be reduced.

B. DECREASE THE ANGLE BETWEEN EXTERNAL DF AND PM'S MAGNETIZATION DIRECTION

When flux lines enter a low magnetic permeability environment from a high magnetic permeability environment, the flux lines enter the low permeability region vertically. As we know, the counter-magnetization component of the DF is effective in the ID. Therefore, any change in the rotor parameters leading to an increase in the angle between the magnetization direction of the magnet and the direction of the DF can reduce the possibility of ID.

C. INCREASE THE DISTANCE BETWEEN EXTERNAL DF AND PMs

To demagnetize the PMs, DF must reach the PMs. the larger distance between the PMs and the source of DF, the lower probability of the ID will be. Consequently, any geometry modification increasing the distance between the PMs and the source of DF or blocking the DF to reach the PMs can reduce the probability of ID.

D. DECREASE THE EDDY CURRENT LOSS IN THE PMs BY DIVIDING THE PMs

By dividing the PMs, the eddy current losses and the working temperature of the PMs are decreased and consequently, the risk of ID will be weakened.

VIII. CONCLUSION

In this paper, a comprehensive review of ID has been presented. Four critical aspects in the proper design and validation of PM machines in terms of ID, including the PM modelling methods, ID analysis model, design optimization methods, and experimental setups, have been surveyed. The advantages and disadvantages of the existing techniques in these areas have been highlighted. Furthermore, design tips towards the design of ID fault-tolerant PM machines and other research opportunities to enhance the reliability of PMs machines are also presented.

In dealing with the ID phenomenon, using the developed PM model, required computational complexity, parameter extraction, temperature variation characteristics, and accurate modelling of the knee point are essential aspects of applying these modelling methods. Regarding the ID analysis model, although the FEM analysis model can accurately model the ID in PM machines, its high computational time and memory required restricts its application to the initial stage design of the PM machines. On the other hand, other ID analysis models were not developed entirely and cannot accurately model the partial ID. Therefore, the need for a developed analytical ID analysis model is obvious and requires more attention. Generally, ID-tolerant capability of the designed PM machines is evaluated after finalizing the design. There is a lack in this area, and it requires developing optimisation methods that can consider ID in the design stage.

Overall, the gathered information in this paper for different aspects of the modeling, design, optimization, and experimental verifications of the PM machines in terms of ID will be a good source for the designer of the PM machines to avoid ID.

REFERENCES

[1] F. Mahmouditabar, A. Vahedi, and N. Takorabet, "Design and analysis of interior permanent magnet motor for electric vehicle application considering irreversible demagnetization," *IEEE Trans. Ind. Appl.*, vol. 58, no. 1, pp. 284–293, Jan. 2022, doi: 10.1109/TIA.2021.3126695.

[2] X. Fan, B. Zhang, R. Qu, D. Li, J. Li, and Y. Huo, "Comparative thermal analysis of IPMSMs with integral-slot distributed-winding (ISDW) and fractional-slot concentrated-winding (FSCW) for electric vehicle application," *IEEE Trans. Ind. Appl.*, vol. 55, no. 4, pp. 3577–3588, Jul. 2019, doi: 10.1109/TIA.2019.2903187.

[3] G. J. Li, B. Ren, Z. Q. Zhu, M. P. Foster, and D. A. Stone, "Demagnetization withstand capability enhancement of surface mounted PM machines using stator modularity," *IEEE Trans. Ind. Appl.*, vol. 54, no. 2, pp. 1302–1311, Mar. 2018, doi: 10.1109/TIA.2017.2777922.

[4] M. Baranski, W. Szelag, and W. Lyskawinski, "Analysis of the partial demagnetization process of magnets in a line start permanent magnet synchronous motor," *Energies*, vol. 13, no. 21, p. 5562, Oct. 2020, doi: 10.3390/EN13215562.

[5] T. A. Huynh, J.-X. Peng, M.-F. Hsieh, and P.-W. Huang, "Anti-demagnetization analysis of fractional slot concentrated windings interior permanent magnet motor considering effect of rotor design parameters," *IEEE Trans. Magn.*, vol. 58, no. 2, pp. 1–6, Feb. 2022, doi: 10.1109/TMAG.2021.3090319.

[6] M. Wang, H. Zhu, C. Zhou, P. Zheng, and C. Tong, "Analysis and optimization of a V-shape combined pole interior permanent-magnet synchronous machine with temperature rise and demagnetization considered," *IEEE Access*, vol. 9, pp. 64761–64775, 2021, doi: 10.1109/ACCESS.2021.3076228.

[7] Q. Ma, A. El-Refaie, and B. Lequesne, "Low-cost interior permanent magnet machine with multiple magnet types," *IEEE Trans. Ind. Appl.*, vol. 56, no. 2, pp. 1452–1463, Mar. 2020, doi: 10.1109/TIA.2020.2966458.

[8] J. Faiz and H. Nejadi-Koti, "Demagnetization fault indexes in permanent magnet synchronous motors—An overview," *IEEE Trans. Magn.*, vol. 52, no. 4, pp. 1–11, Apr. 2016, doi: 10.1109/TMAG.2015.2480379.

[9] S. S. Moosavi, A. Djerdir, Y. A. Amirat, and D. A. Khaburi, "Demagnetization fault diagnosis in permanent magnet synchronous motors: A review of the state-of-the-art," *J. Magn. Magn. Mater.*, vol. 391, pp. 203–212, Oct. 2015, doi: 10.1016/J.JMMM.2015.04.062.

[10] J. Faiz and E. Mazaheri-Tehrani, "Demagnetization modeling and fault diagnosing techniques in permanent magnet machines under stationary and nonstationary conditions: An overview," *IEEE Trans. Ind. Appl.*, vol. 53, no. 3, pp. 2772–2785, May 2017, doi: 10.1109/TIA.2016.2608950.

[11] W. Bekir, O. Messal, and A. Benabou, "Permanent magnet nonlinear demagnetization model for FEM simulation environment," *IEEE Trans. Magn.*, vol. 58, no. 2, pp. 1–5, Feb. 2022, doi: 10.1109/TMAG.2021.3084445.

[12] S. Ruoho, E. Dlala, and A. Arkkio, "Comparison of demagnetization models for finite-element analysis of permanent-magnet synchronous machines," *IEEE Trans. Magn.*, vol. 43, no. 11, pp. 3964–3968, Nov. 2007, doi: 10.1109/TMAG.2007.906749.

[13] J. Chen, D. Wang, S. Cheng, Y. Jiang, X. Teng, Z. Chen, Y. Shen, F. Birnkammer, and D. Gerling, "A hysteresis model based on linear curves for NdFeB permanent magnet considering temperature effects," *IEEE Trans. Magn.*, vol. 54, no. 3, pp. 1–5, Mar. 2018, doi: 10.1109/TMAG.2017.2763238.

[14] A. Bergqvist, D. Lin, and P. Zhou, "Temperature-dependent vector hysteresis model for permanent magnets," *IEEE Trans. Magn.*, vol. 50, no. 2, pp. 345–348, Feb. 2014, doi: 10.1109/TMAG.2013.2282822.

[15] D. Egorov, I. Petrov, J. Link, H. Kankaanpää, R. Stern, and J. J. Pyrhönen, "Linear recoil curve demagnetization models for rare-earth magnets in electrical machines," in *Proc. 45th Annu. Conf. IEEE Ind. Electron. Soc. (IECON)*, vol. 1, Oct. 2019, pp. 1157–1164, doi: 10.1109/IECON.2019.8927388.

[16] W. Li, G. Feng, C. Lai, Z. Li, J. Tian, and N. C. Kar, "Demagnetization analysis of interior permanent magnet machines under integrated charging operation," *IEEE Trans. Ind. Appl.*, vol. 55, no. 5, pp. 5204–5213, Sep. 2019, doi: 10.1109/TIA.2019.2922209.

[17] S. Hamidizadeh, N. Alatawneh, R. R. Chromik, and D. A. Lowther, "Comparison of different demagnetization models of permanent magnet in machines for electric vehicle application," *IEEE Trans. Magn.*, vol. 52, no. 5, pp. 1–4, May 2016, doi: 10.1109/TMAG.2015.2513067.

[18] D. Egorov, I. Petrov, J. Pyrhonen, J. Link, and R. Stern, "Linear recoil curve demagnetization models for ferrite magnets in rotating machinery," in *Proc. 43rd Annu. Conf. IEEE Ind. Electron. Soc. (IECON)*, Oct. 2017, pp. 2046–2062, doi: 10.1109/IECON.2017.8216344.

[19] S. Zhu, M. Cheng, W. Hua, X. Cai, and M. Tong, "Finite element analysis of flux-switching PM machine considering oversaturation and irreversible demagnetization," *IEEE Trans. Magn.*, vol. 51, no. 11, pp. 1–4, Nov. 2015, doi: 10.1109/TMAG.2015.2445774.

[20] L. Guo, C. Xia, H. Wang, Z. Wang, and T. Shi, "Improved equivalent magnetic network modeling for analyzing working points of PMs in interior permanent magnet machine," *J. Magn. Magn. Mater.*, vol. 454, pp. 39–50, May 2018, doi: 10.1016/j.jmmm.2018.01.018.

[21] B. Guo, Y. Huang, F. Peng, and J. Dong, "General analytical modeling for magnet demagnetization in surface mounted permanent magnet machines," *IEEE Trans. Ind. Electron.*, vol. 66, no. 8, pp. 5830–5838, Aug. 2019, doi: 10.1109/TIE.2018.2873099.

[22] D. Torregrossa, A. Khoobroo, and B. Fahimi, "Prediction of acoustic noise and torque pulsation in PM synchronous machines with static eccentricity and partial demagnetization using field reconstruction method," *IEEE Trans. Ind. Electron.*, vol. 59, no. 2, pp. 934–944, Feb. 2012, doi: 10.1109/TIE.2011.2151810.

[23] T. Ishikawa, Y. Seki, and N. Kurita, "Analysis for fault detection of vector-controlled permanent magnet synchronous motor with permanent magnet defect," *IEEE Trans. Magn.*, vol. 49, no. 5, pp. 2331–2334, May 2013, doi: 10.1109/TMAG.2013.2243135.

[24] P. Madina, J. Poza, G. Ugalde, and G. Almandoz, "Analysis of non-uniform circumferential segmentation of magnets to reduce eddy-current losses in SPMSM machines," in *Proc. 20th Int. Conf. Electr. Mach. (ICEM)*, Sep. 2012, pp. 79–84, doi: 10.1109/ICElMach.2012.6349843.

[25] B.-C. Kim, J.-H. Lee, and D.-W. Kang, "A study on the effect of eddy current loss and demagnetization characteristics of magnet division," *IEEE Trans. Appl. Supercond.*, vol. 30, no. 4, pp. 1–5, Jun. 2020, doi: 10.1109/TASC.2020.2986967.

[26] Y. Shen, Z. Zeng, Q. Lu, and L. Wu, "Design optimization and performance investigation of linear doubly salient slot permanent magnet machines," *IEEE Trans. Ind. Appl.*, vol. 55, no. 2, pp. 1524–1535, Mar. 2019, doi: 10.1109/TIA.2018.2885329.

[27] D. Fan, X. Zhu, L. Quan, and Z. Xiang, "Dynamic demagnetisation investigation for less-rare-earth flux switching permanent magnet motors considering three-phase short-circuit fault," *IET Electr. Power Appl.*, vol. 12, no. 8, pp. 1176–1182, Sep. 2018, doi: 10.1049/iet-epa.2018.0002.

[28] Y. Kong, M. Lin, M. Yin, and L. Hao, "Rotor structure on reducing demagnetization of magnet and torque ripple in a PMa-synRM with ferrite permanent magnet," *IEEE Trans. Magn.*, vol. 54, no. 11, pp. 1–5, Nov. 2018, doi: 10.1109/TMAG.2018.2827104.

[29] G. Park, J. Kim, B. Son, and S. Jung, "Optimal design of PMa-synRM for an electric propulsion system considering wide operation range and demagnetization," *IEEE Trans. Appl. Supercond.*, vol. 28, no. 3, pp. 1–4, Apr. 2018, doi: 10.1109/TASC.2018.2807375.

[30] J.-C. Urresty, J.-R. Riba, and L. Romeral, "A back-emf based method to detect magnet failures in PMSMs," *IEEE Trans. Magn.*, vol. 49, no. 1, pp. 591–598, Jan. 2013, doi: 10.1109/TMAG.2012.2207731.

[31] C. Ruschetti, C. Verucchi, G. Bossio, C. De Angelo, and G. García, "Rotor demagnetization effects on permanent magnet synchronous machines," *Energy Convers. Manage.*, vol. 74, pp. 1–8, Oct. 2013, doi: 10.1016/J.ENCONMAN.2013.05.001.

[32] K. Lee, W. Kim, C. Jin, and J. Lee, "Local demagnetisation analysis of a permanent magnet motor," *IET Electr. Power Appl.*, vol. 9, no. 3, pp. 280–286, Mar. 2015, doi: 10.1049/IET-EPA.2014.0244.

[33] G. Choi, Y. Zhang, and T. M. Jahns, "Experimental verification of rotor demagnetization in a fractional-slot concentrated-winding PM synchronous machine under drive fault conditions," *IEEE Trans. Ind. Appl.*, vol. 53, no. 4, pp. 3467–3475, Jul. 2017, doi: 10.1109/TIA.2017.2686806.

[34] Y. Zhilichev, "Analysis of permanent magnet demagnetization accounting for minor *B-H* curves," *IEEE Trans. Magn.*, vol. 44, no. 11, pp. 4285–4288, Nov. 2008, doi: 10.1109/TMAG.2008.2001343.

[35] K. H. J. Buschow and F. R. de Boer, "Physics of magnetism and magnetic materials," in *Physics of Magnetism and Magnetic Materials*. New York, NY, USA: Springer, 2003, doi: 10.1007/B100503.

[36] J. M. D. Coey, "Magnetism and magnetic materials," *Magn. Magn. Mater.*, vol. 9780521816144, pp. 1–617, Jan. 2010, doi: 10.1017/CBO9780511845000.

[37] E. S. Hamdi, "Design of small electrical machines," Grades Ferrite, Bunting–Berkhamsted, Berkhamsted, U.K., Tech. Rep., 1994, p. 260. [Online]. Available: https://e-magnetsuk.com/ferrite-magnets/grades-of-ferrite/

[38] *Grades of Ferrite | Bunting—eMagnets*. Accessed: Mar. 11, 2023. [Online]. Available: https://e-magnetsuk.com/ferrite-magnets/grades-of-ferrite/

[39] *K&J Magnetics—Demagnetization Curves*. Accessed: Mar. 11, 2023. [Online]. Available: https://www.kjmagnetics.com/bhcurves.asp
[40] F. Mahmouditabar, A. Vahedi, and P. Ojaghlu, "Investigation of demagnetization effect in an interior V-shaped magnet synchronous motor at dynamic and static conditions," *Iranian J. Electr. Electron. Eng.*, vol. 14, no. 1, pp. 22–27, Mar. 2018, doi: 10.22068/IJEEE.14.1.22.
[41] F. Mahmouditabar, A. Vahedi, and P. Ojaghlu, "Investigation of demagnetization phenomenon in novel ring winding AFPM motor with modified algorithm," *J. Magn. Magn. Mater.*, vol. 491, Dec. 2019, Art. no. 165539, doi: 10.1016/j.jmmm.2019.165539.
[42] R. Sami, "Modeling demagnetization of sintered NdFeB magnet material in time-discretized finite element analysis," Ph.D. dissertation, School Elect. Eng., Aalto Univ., Espoo, Finland, Jan. 2011. [Online]. Available: http://lib.tkk.fi/Diss/2011/isbn9789526040011/isbn9789526040011.pdf
[43] M. Rosu, J. Saitz, and A. Arkkio, "Hysteresis model for finite-element analysis of permanent-magnet demagnetization in a large synchronous motor under a fault condition," *IEEE Trans. Magn.*, vol. 41, no. 6, pp. 2118–2123, Jun. 2005, doi: 10.1109/TMAG.2005.848319.
[44] E. Dlala, J. Saitz, and A. Arkkio, "Inverted and forward Preisach models for numerical analysis of electromagnetic field problems," *IEEE Trans. Magn.*, vol. 42, no. 8, pp. 1963–1973, Aug. 2006, doi: 10.1109/TMAG.2006.877463.
[45] J. H. Lee and J. P. Hong, "Permanent magnet demagnetization characteristic analysis of a variable flux memory motor using coupled Preisach modeling and FEM," *IEEE Trans. Magn.*, vol. 44, no. 6, pp. 1550–1553, Jun. 2008, doi: 10.1109/TMAG.2007.916093.
[46] C. Yu, S. Niu, S. Lau Ho, W. Fu, and L. Li, "Hysteresis modeling in transient analysis of electric motors with AlNiCo magnets," *IEEE Trans. Magn.*, vol. 51, no. 3, pp. 1–4, Mar. 2015, doi: 10.1109/TMAG.2014.2362615.
[47] F. Mahmouditabar, A. Vahedi, P. Ojaghlu, and N. Takorabet, "Irreversible demagnetization analysis of RWAFPM motor using modified MEC algorithm," *COMPEL-Int. J. Comput. Math. Electr. Electron. Eng.*, vol. 39, no. 5, pp. 1227–1239, Jul. 2020, doi: 10.1108/COMPEL-01-2020-0021.
[48] P. Zhou, D. Lin, Y. Xiao, N. Lambert, and M. A. Rahman, "Temperature-dependent demagnetization model of permanent magnets for finite element analysis," *IEEE Trans. Magn.*, vol. 48, no. 2, pp. 1031–1034, Feb. 2012, doi: 10.1109/TMAG.2011.2172395.
[49] J. S. Hsu, C. W. Ayers, C. L. Coomer, R. H. Wiles, S. L. Campbell, K. T. Lowe, and R. T. Michelhaugh, "Report on Toyota/Prius motor torque capability, torque property, no-load back EMF, and mechanical losses," Oak Ridge Inst. Sci. Educ., Oak Ridge, TN, USA, Tech. Rep. ORNL/TM-2004/185, May 2007. [Online]. Available: https://info.ornl.gov/sites/publications/Files/Pub57343.pdf
[50] H. Yang, W. Liu, H. Zheng, H. Lin, Z. Q. Zhu, F. Peng, Y. Li, S. Lyu, and X. Huang, "A novel delta-type hybrid-magnetic-circuit variable flux memory machine for electrified vehicle applications," *IEEE Trans. Transport. Electrific.*, vol. 8, no. 3, pp. 3512–3523, Sep. 2022, doi: 10.1109/TTE.2022.3152894.
[51] D.-W. Kang, "Analysis of vibration and performance considering demagnetization phenomenon of the interior permanent magnet motor," *IEEE Trans. Magn.*, vol. 53, no. 11, pp. 1–7, Nov. 2017, doi: 10.1109/TMAG.2017.2708421.
[52] M. Seo, T. Lee, Y. Ko, Y. Kim, and S. Jung, "Irreversible demagnetization analysis with respect to winding connection and current ripple in brushless DC motor," *IEEE Trans. Appl. Supercond.*, vol. 28, no. 3, pp. 1–4, Apr. 2018, doi: 10.1109/TASC.2018.2792449.
[53] Y.-S. Lee, K.-T. Kim, and J. Hur, "Finite-element analysis of the demagnetization of IPM-type BLDC motor with stator turn fault," *IEEE Trans. Magn.*, vol. 50, no. 2, pp. 889–892, Feb. 2014, doi: 10.1109/TMAG.2013.2283498.
[54] H. Chen, R. Qu, J. Li, and D. Li, "Demagnetization performance of a 7 MW interior permanent magnet wind generator with fractional-slot concentrated windings," *IEEE Trans. Magn.*, vol. 51, no. 11, pp. 1–4, Nov. 2015, doi: 10.1109/TMAG.2015.2442263.
[55] V. I. Patel, J. Wang, and S. S. Nair, "Demagnetization assessment of fractional-slot and distributed wound 6-phase permanent magnet machines," *IEEE Trans. Magn.*, vol. 51, no. 6, pp. 1–11, Jun. 2015, doi: 10.1109/TMAG.2014.2380152.
[56] P. Peng, H. Xiong, J. Zhang, W. Li, F. Leonardi, C. Rong, M. W. Degner, F. Liang, and L. Zhu, "Effects of external field orientation on permanent magnet demagnetization," *IEEE Trans. Ind. Appl.*, vol. 53, no. 4, pp. 3438–3446, Jul. 2017, doi: 10.1109/TIA.2017.2686344.
[57] J. D. McFarland and T. M. Jahns, "Influence of d- and q-axis currents on demagnetization in PM synchronous machines," in *Proc. IEEE Energy Convers. Congr. Expo. (ECCE)*, Sep. 2013, pp. 4380–4387, doi: 10.1109/ECCE.2013.6647286.
[58] L. Wu, Y. Du, Z. Chen, Y. Guo, H. Wen, and Y. Fang, "Influence of load characteristics on three-phase short circuit and demagnetization of surface-mounted PM synchronous motor," *IEEE Trans. Ind. Appl.*, vol. 56, no. 3, pp. 2427–2440, May 2020, doi: 10.1109/TIA.2020.2968036.
[59] S. Wu, S. Wu, W. Zhao, and S. Cui, "Demagnetization research on PMs in the Halbach magnetized pulsed alternator," *CES Trans. Electr. Mach. Syst.*, vol. 3, no. 2, pp. 170–177, Jun. 2019, doi: 10.30941/CESTEMS.2019.00023.
[60] R. Alipour-Sarabi, Z. Nasiri-Gheidari, and H. Oraee, "Development of a three-dimensional magnetic equivalent circuit model for axial flux machines," *IEEE Trans. Ind. Electron.*, vol. 67, no. 7, pp. 5758–5767, Jul. 2020, doi: 10.1109/TIE.2019.2934065.
[61] Y. Liu, L. Li, Q. Gao, J. Cao, and Z. Sun, "An analytical model and optimization of a novel hybrid rotor machine for high torque density," *IEEE Trans. Energy Convers.*, vol. 36, no. 1, pp. 230–241, Mar. 2021, doi: 10.1109/TEC.2020.3008768.
[62] H. Saneie and Z. Nasiri-Gheidari, "Performance analysis of outer-rotor single-phase induction motor based on magnetic equivalent circuit," *IEEE Trans. Ind. Electron.*, vol. 68, no. 2, pp. 1046–1054, Feb. 2021, doi: 10.1109/TIE.2020.2969125.
[63] P. Naderi and M. Heidary, "A novel permanent magnet flux-switching linear motor performance analysis by flexible MEC method," *IEEE Trans. Energy Convers.*, vol. 36, no. 3, pp. 1910–1918, Sep. 2021, doi: 10.1109/TEC.2020.3046139.
[64] P. Ojaghlu, A. Vahedi, and F. Totoonchian, "Magnetic equivalent circuit modelling of ring winding axial flux machine," *IET Electr. Power Appl.*, vol. 12, no. 3, pp. 293–300, Mar. 2018, doi: 10.1049/iet-epa.2017.0517.
[65] Y. Huang, T. Zhou, J. Dong, H. Lin, H. Yang, and M. Cheng, "Magnetic equivalent circuit modeling of yokeless axial flux permanent magnet machine with segmented armature," *IEEE Trans. Magn.*, vol. 50, no. 11, pp. 1–4, Nov. 2014, doi: 10.1109/TMAG.2014.2322874.
[66] S. Li, Y. Li, and B. Sarlioglu, "Partial irreversible demagnetization assessment of flux-switching permanent magnet machine using ferrite permanent magnet material," *IEEE Trans. Magn.*, vol. 51, no. 7, pp. 1–9, Jul. 2015, doi: 10.1109/TMAG.2015.2405898.
[67] C.-L. Jeong and J. Hur, "Optimization design of PMSM with hybrid-type permanent magnet considering irreversible demagnetization," *IEEE Trans. Magn.*, vol. 53, no. 11, pp. 1–4, Nov. 2017, doi: 10.1109/TMAG.2017.2707102.
[68] D. Momma, Y. Yoshida, and K. Tajima, "Demagnetization analysis of ferrite magnet motor based on reluctance network analysis," in *Proc. 19th Int. Conf. Elect. Mach. Syst. (ICEMS)*, Nov. 2016, pp. 1–6. Accessed: Jul. 13, 2022. [Online]. Available: https://ieeexplore.ieee.org/document/7837515
[69] T. Raminosoa, J. A. Farooq, A. Djerdir, and A. Miraoui, "Reluctance network modelling of surface permanent magnet motor considering iron nonlinearities," *Energy Convers. Manage.*, vol. 50, no. 5, pp. 1356–1361, May 2009, doi: 10.1016/J.ENCONMAN.2009.01.012.
[70] L. Guo, C. Xia, H. Wang, Z. Wang, and T. Shi, "Improved equivalent magnetic network modeling for analyzing working points of PMs in interior permanent magnet machine," *J. Magn. Magn. Mater.*, vol. 454, pp. 39–50, May 2018, doi: 10.1016/J.JMMM.2018.01.018.
[71] W. Sun, Q. Li, L. Sun, and X. Jiang, "Study on magnetic shielding for performance improvement of axial-field dual-rotor segmented switched reluctance machine," *CES Trans. Electr. Mach. Syst.*, vol. 5, no. 1, pp. 50–61, Mar. 2021, doi: 10.30941/CESTEMS.2021.00007.
[72] M. Niazazari, M. Mirsalim, and S. Mohammadi, "Analytical framework for analysis and demagnetization study of a slotted solid-rotor line-start permanent-magnet synchronous motor," in *Proc. 5th Annu. Int. Power Electron., Drive Syst. Technol. Conf. (PEDSTC)*, Feb. 2014, pp. 494–499, doi: 10.1109/PEDSTC.2014.6799425.
[73] E. Ajily, M. Ardebili, and K. Abbaszadeh, "Magnet defect and rotor eccentricity modeling in axial-flux permanent-magnet machines via 3-D field reconstruction method," *IEEE Trans. Energy Convers.*, vol. 31, no. 2, pp. 486–495, Jun. 2016, doi: 10.1109/TEC.2015.2506819.
[74] J. De Bisschop, P. Sergeant, A. Hemeida, H. Vansompel, and L. Dupre, "Analytical model for combined study of magnet demagnetization and eccentricity defects in axial flux permanent magnet synchronous machines," *IEEE Trans. Magn.*, vol. 53, no. 9, pp. 1–12, Sep. 2017, doi: 10.1109/TMAG.2017.2709267.

[75] J. A. Farooq, A. Djerdir, and A. Miraoui, "Analytical modeling approach to detect magnet defects in permanent-magnet brushless motors," *IEEE Trans. Magn.*, vol. 44, no. 12, pp. 4599–4604, Dec. 2008, doi: 10.1109/TMAG.2008.2001751.
[76] B. Lee, J. Jung, and J. Hong, "An improved analysis method of irreversible demagnetization for a single-phase line-start permanent magnet motor," *IEEE Trans. Magn.*, vol. 54, no. 11, pp. 1–5, Nov. 2018, doi: 10.1109/TMAG.2018.2828507.
[77] M. Baranski, W. Szelag, and W. Lyskawinski, "Experimental and simulation studies of partial demagnetization process of permanent magnets in electric motors," *IEEE Trans. Energy Convers.*, vol. 36, no. 4, pp. 3137–3145, Dec. 2021, doi: 10.1109/TEC.2021.3082903.
[78] Md. Z. Islam, A. Arafat, S. S. R. Bonthu, and S. Choi, "Design of a robust five-phase ferrite-assisted synchronous reluctance motor with low demagnetization and mechanical deformation," *IEEE Trans. Energy Convers.*, vol. 34, no. 2, pp. 722–730, Jun. 2019, doi: 10.1109/TEC.2018.2882780.
[79] Y. Zhang, S. McLoone, and W. Cao, "Electromagnetic loss modeling and demagnetization analysis for high speed permanent magnet machine," *IEEE Trans. Magn.*, vol. 54, no. 3, pp. 1–5, Mar. 2018, doi: 10.1109/TMAG.2017.2759247.
[80] J. De Bisschop, A. Abdallh, P. Sergeant, and L. Dupre, "Identification of demagnetization faults in axial flux permanent magnet synchronous machines using an inverse problem coupled with an analytical model," *IEEE Trans. Magn.*, vol. 50, no. 11, pp. 1–4, Nov. 2014, doi: 10.1109/TMAG.2014.2316851.
[81] L. Ye, M. Cao, Y. Liu, and D. Li, "Multi-field coupling analysis and demagnetization experiment of permanent magnet retarder for heavy vehicles," *IEEE Access*, vol. 7, pp. 50734–50745, 2019, doi: 10.1109/ACCESS.2018.2884236.
[82] M. Galea, L. Papini, H. Zhang, C. Gerada, and T. Hamiti, "Demagnetization analysis for Halbach array configurations in electrical machines," *IEEE Trans. Magn.*, vol. 51, no. 9, pp. 1–9, Sep. 2015, doi: 10.1109/TMAG.2015.2429645.
[83] A. Nobahari, A. Vahedi, and R. Nasiri-Zarandi, "A modified permanent magnet-assisted synchronous reluctance motor design for torque characteristics improvement," *IEEE Trans. Energy Convers.*, vol. 37, no. 2, pp. 989–998, Jun. 2022, doi: 10.1109/TEC.2021.3127081.
[84] X. Sun, Z. Shi, Y. Cai, G. Lei, Y. Guo, and J. Zhu, "Driving-cycle-oriented design optimization of a permanent magnet hub motor drive system for a four-wheel-drive electric vehicle," *IEEE Trans. Transport. Electrific.*, vol. 6, no. 3, pp. 1115–1125, Sep. 2020, doi: 10.1109/TTE.2020.3009396.
[85] Z. Shi, X. Sun, Y. Cai, and Z. Yang, "Robust design optimization of a five-phase PM hub motor for fault-tolerant operation based on Taguchi method," *IEEE Trans. Energy Convers.*, vol. 35, no. 4, pp. 2036–2044, Dec. 2020, doi: 10.1109/TEC.2020.2989438.
[86] X. Sun, N. Xu, and M. Yao, "Sequential subspace optimization design of a dual three-phase permanent magnet synchronous hub motor based on NSGA III," *IEEE Trans. Transport. Electrific.*, vol. 9, no. 1, pp. 622–630, Mar. 2023, doi: 10.1109/TTE.2022.3190536.
[87] K. Yamazaki and A. Abe, "Loss investigation of interior permanent-magnet motors considering carrier harmonics and magnet eddy currents," *IEEE Trans. Ind. Appl.*, vol. 45, no. 2, pp. 659–665, 2009, doi: 10.1109/TIA.2009.2013550.
[88] K. Kondo, S. Kusase, T. Maekawa, and K. Hanada, "A new PM-assisted synchronous reluctance motor with three-dimensional trench air gap," *IEEE Trans. Ind. Appl.*, vol. 50, no. 4, pp. 2485–2492, Jul. 2014, doi: 10.1109/TIA.2013.2297446.
[89] G. Li, P. Taras, Z. Zhu, J. Ojeda, and M. Gabsi, "Investigation of irreversible demagnetisation in switched flux permanent magnet machines under short-circuit conditions," *IET Electr. Power Appl.*, vol. 11, no. 4, pp. 595–602, Apr. 2017, doi: 10.1049/IET-EPA.2016.0189.
[90] W. Wang, P. Zheng, M. Wang, Y. Liu, Z. Fu, and Y. Sui, "Demagnetization and permanent-magnet minimization analyses of less-rare-earth interior permanent-magnet synchronous machines used for electric vehicles," *IEEE Trans. Magn.*, vol. 54, no. 11, pp. 1–5, Nov. 2018, doi: 10.1109/TMAG.2018.2840527.
[91] T. Wang, X. Zhu, S. Zheng, L. Quan, Z. Xiang, and X. Zhou, "Investigation on torque characteristic and PM operation point of flux-intensifying PM motor considering low-speed operation," *IEEE Trans. Magn.*, vol. 57, no. 2, pp. 1–5, Feb. 2021, doi: 10.1109/TMAG.2020.3019299.
[92] S. Lyu, H. Yang, H. Lin, Z. Q. Zhu, H. Zheng, and Z. Pan, "Influence of design parameters on on-load demagnetization characteristics of switched flux hybrid magnet memory machine," *IEEE Trans. Magn.*, vol. 55, no. 7, pp. 1–5, Jul. 2019, doi: 10.1109/TMAG.2019.2903160.
[93] J. Dong, Y. Huang, L. Jin, and H. Lin, "Comparative study of surface-mounted and interior permanent-magnet motors for high-speed applications," *IEEE Trans. Appl. Supercond.*, vol. 26, no. 4, pp. 1–4, Jun. 2016, doi: 10.1109/TASC.2016.2514342.
[94] K.-C. Kim, K. Kim, H. J. Kim, and J. Lee, "Demagnetization analysis of permanent magnets according to rotor types of interior permanent magnet synchronous motor," *IEEE Trans. Magn.*, vol. 45, no. 6, pp. 2799–2802, Jun. 2009, doi: 10.1109/TMAG.2009.2018661.
[95] G. Choi, "Analysis and experimental verification of the demagnetization vulnerability in various PM synchronous machine configurations for an EV application," *Energies*, vol. 14, no. 17, p. 5447, Sep. 2021, doi: 10.3390/EN14175447.
[96] C. Diao, W. Zhao, N. Wang, and X. Wang, "Analysis of a high-speed axial flux permanent magnet synchronous motor with cost-effective hybrid magnets," *IEEE Trans. Magn.*, vol. 59, no. 5, pp. 1–4, May 2023, doi: 10.1109/TMAG.2023.3241183.
[97] F. Mahmouditabar, A. Vahedi, and N. Takorabet, "Demagnetisation optimisation of ring winding axial flux permanent magnet motor by modifying the load line of the magnet," *IET Electr. Power Appl.*, Mar. 2023, doi: 10.1049/ELP2.12314.
[98] A. Rehman and B. Kim, "Characteristics analysis of consequent-pole ferrite magnet Vernier machine using novel equivalent magnetic circuit," *IEEE J. Emerg. Sel. Topics Power Electron.*, vol. 10, no. 2, pp. 1823–1833, Apr. 2022, doi: 10.1109/JESTPE.2021.3072940.
[99] H. Yang, S. Lyu, H. Lin, Z. Zhu, H. Zheng, and T. Wang, "A novel hybrid-magnetic-circuit variable flux memory machine," *IEEE Trans. Ind. Electron.*, vol. 67, no. 7, pp. 5258–5268, Jul. 2020, doi: 10.1109/TIE.2019.2931494.
[100] C. Jeong, Y. Kim, and J. Hur, "Optimized design of PMSM with hybrid-type permanent magnet for improving performance and reliability," *IEEE Trans. Ind. Appl.*, vol. 55, no. 5, pp. 4692–4701, Sep. 2019, doi: 10.1109/TIA.2019.2924614.
[101] F. Mahmouditabar and A. Vahedi, "Optimum design of FSPM motor for small water pump application considering irreversible demagnetization," *Iranian J. Sci. Technol., Trans. Electr. Eng.*, vol. 45, no. 3, pp. 777–788, Jan. 2021, doi: 10.1007/S40998-020-00394-6.
[102] K.-Y. Yoon and K.-Y. Hwang, "Optimal design of spoke-type IPM motor allowing irreversible demagnetization to minimize PM weight," *IEEE Access*, vol. 9, pp. 65721–65729, 2021, doi: 10.1109/ACCESS.2021.3070747.
[103] K.-Y. Hwang and K.-Y. Yoon, "Fault-tolerant design process of spoke-type IPM motor considering irreversible demagnetization of PM in integrated electric brake system," *IEEE Trans. Magn.*, vol. 58, no. 11, pp. 1–9, Nov. 2022, doi: 10.1109/TMAG.2022.3202098.
[104] W. L. Roux, R. G. Harley, and T. G. Habetler, "Detecting rotor faults in low power permanent magnet synchronous machines," *IEEE Trans. Power Electron.*, vol. 22, no. 1, pp. 322–328, Jan. 2007, doi: 10.1109/TPEL.2006.886620.
[105] K.-T. Kim, Y.-S. Lee, and J. Hur, "Transient analysis of irreversible demagnetization of permanent-magnet brushless DC motor with interturn fault under the operating state," *IEEE Trans. Ind. Appl.*, vol. 50, no. 5, pp. 3357–3364, Sep. 2014, doi: 10.1109/TIA.2014.2311494.
[106] T. H. Akinaga, T. Staudt, P. E. da Silva, and A. A. Espindola, "FEA-based method for estimating PM demagnetization in electrical motor design: Development and experimental validation," in *Proc. 22nd Int. Conf. Electr. Mach. (ICEM)*, Sep. 2016, pp. 1749–1755, doi: 10.1109/ICELMACH.2016.7732760.
[107] G. Almandoz, I. Gómez, G. Ugalde, J. Poza, and A. J. Escalada, "Study of demagnetization risk in PM machines," *IEEE Trans. Ind. Appl.*, vol. 55, no. 4, pp. 3490–3500, Jul. 2019, doi: 10.1109/TIA.2019.2904459.
[108] J.-K. Kang and J. Hur, "Fault mechanism analysis of irreversible demagnetization due to the dynamic eccentricity of IPMSM for EV traction," *IEEE Access*, vol. 10, pp. 64483–64494, 2022, doi: 10.1109/ACCESS.2022.3183347.
[109] P. Peng, J. Zhang, W. Li, F. Leonardi, C. Rong, M. W. Degner, F. Liang, and L. Zhu, "Time-dependent demagnetization of NdFeB magnets under DC and pulsed magnetic fields," *IEEE Trans. Magn.*, vol. 56, no. 3, pp. 1–10, Mar. 2020, doi: 10.1109/TMAG.2020.2966572.

FARSHID MAHMOUDITABAR received the B.Sc. degree in electrical engineering from Shahrekord University, Shahrekord, Iran, in 2016, and the M.Sc. and Ph.D. degrees in electrical engineering from the Iran University of Science and Technology, Tehran, Iran, in 2018 and 2021, respectively. From 2019 to 2021, he was an Electrical Machine and Powertrain Engineer with IKCO, where he designed and manufactured several water-cooled IM for EV applications. From 2021 to 2023, he was an Electrical Machine and Powertrain Engineer with MAPNA Locomotive company, where he designed and developed the electrical machines for diesel-electric and overhead-powered electric locomotives. In 2023, he joined Newcastle University as a Research Associate working on the design of electrical machines for manufacture. His main research interests include the design, modeling, and optimization of electrical machines.

ABOLFAZL VAHEDI (Senior Member, IEEE) was born in Tehran, Iran, in 1966. He received the B.S. degree in electrical engineering from Ferdowsi University, Mashhad, Iran, in 1989, and the M.Sc. and Ph.D. degrees in electrical engineering from the National Polytechnic Institute of Lorraine, Nancy, France, in 1992 and 1996, respectively. He is currently a Professor with the Department of Electrical Engineering, Iran University of Science and Technology, Tehran, where he is the Head of the Special Machines and Drives Laboratory. His current research interests include the design, modeling, optimization, and fault detection of electric machines and drives.

FABRIZIO MARIGNETTI (Senior Member, IEEE) received the Laurea (Hons.) and Ph.D. degrees in electrical engineering from the University of Naples Federico II, in 1993 and 1998, respectively. In 1998, he joined the University of Cassino and Southern Lazio, where he has been an Associate Professor of power electronic converters, machines, and electric drives, since 2005. Since 2021, he has been the Coordinator of the Ph.D. Course in ''Models, Methods, and Technologies for Engineering'' with the University of Cassino and Southern Lazio. He is currently the CEO of the university spin-off company LEDA Srl, Laboratory of Advanced Electrodynamics, which he founded in 2009. He is the author or coauthor of 260 publications in his field of research and two international and five national patents. Since 2015, he has been a fellow of the National Institute of Nuclear Physics (INFN). Since 2022, he has been the Chair of the IE Chapter of the IEEE Italy Section and a member of the Workgroup C4.61 of CIGRE.

Open Access funding provided by 'Università degli Studi di Cassino e del Lazio Meridionale' within the CRUI CARE Agreement